Summer 8-3-2010

Constructability Testing of Folded Plate Girders

Luke A. Glaser
University of Nebraska at Lincoln, lglaser3@gmail.com

CONSTRUCTABILITY TESTING OF

FOLDED PLATE GIRDERS

by

Luke A. Glaser

A THESIS

Presented to the Faculty of

The Graduate College at the University of Nebraska

In Partial Fulfillment of Requirements

For the Degree of Master of Science

Major: Civil Engineering

Under the Supervision of Professor Atorod Azizinamini

Lincoln, Nebraska

August, 2010

CONSTRUCTABILITY TESTING OF COMPOSITE FOLDED PLATE GIRDERS

Luke A. Glaser, M.S.

University of Nebraska, 2010

Adviser: Atorod Azizinamini

A new steel girder bridge system was developed at the University of Nebraska. The innovative girder design is a box girder folded from a single steel plate that has a trapezoid shape with an opening on the bottom. The girder has application in short span bridges and accelerated construction situations. The structural performance of the girder requires investigation in all stages of a bridge's lifecycle. This thesis contains descriptions and results from the first two tests from a series of tests developed to evaluate this new girder shape. The objective of these two tests was to investigate the constructability of the girders. During construction a bridge is in its least stable condition and it is important that the bridge components exhibit both adequate strength and stability during this critical stage. To this end, two girders were tested in flexure over a simple span as a non-composite beam simulating the loading the girders would be subjected to during construction.

The results of the two tests indicate that the folded girder as a whole, and its components, provide adequate strength and stability at construction load levels. Failure occurred at loads that were above normal construction load levels and resulted in a

ductile failure mode, which is a well documented benefit of steel components. The girders remained stable through all phases of loading including failure. The top flange was the weakest component of the beam during construction due to its role as a compression element that has a slender and un-braced form. The compression in the top flange caused local buckling in the top flange even at elastic load levels. This was the cause for loss of stiffness and failure in both specimens. Incorporation of a ridge at the center of the top flange of specimens, results of which are not reported in this thesis, proved to resolve this very early buckling issue.

ACKNOWLEDGEMENT

It is a pleasure to thank those who made this thesis possible. I would like to thank Dr. Azizinamini for providing the opportunity to perform this research, and for his guidance and support throughout the project. I also want to thank Aaron Yakel for his regularly sought after assistance and expertise throughout all of the projects that I worked on. I am indebted to my colleagues who helped med complete my research, especially Kyle Burner and Peter Hilsabeck. I would like to thank my family and friends for their support during the last couple of years. This thesis would not have been possible without the support of my loving wife Christina and my son Jack.

Luke Glaser

The university of Nebraska-Lincoln
August, 2010

Table of Contents

List of Figures

List of tables

Chapter

1 Introduction

In the United States, there are nearly 700,000 bridges. Around 45% of those bridges are less than 60 feet (FHWA NBI data). Many of these structures are deficient and need to be repaired or replaced. An innovative girder design has been developed at the National Bridge Research Organization at the University of Nebraska-Lincoln. The girder has application in short span bridges and accelerated construction situations. The innovative girder design is a box girder folded from a steel plate that has a trapezoid shape with an open bottom and will be referred to as a folded plate girder.

The shape of the folded plate girder causes it to have a large amount of lateral stiffness. This stiffness eliminates the need for cross-frames between the girders. The elimination of cross frames from the system is one of the reasons the system is more cost effective

than the traditional I-beam system. The open bottom geometry of the Folded Plate makes the inspection of the Folded Plate system quick and easy compared to traditional box girders. Simplified inspection procedures translate to reduced inspection costs.

The technology used in fabrication is the same that is used in the fabrication of steel utility poles. Because the girder is fabricated using existing technology it should not be an issue to find fabricators with the capability to fabricate these girders.

1.1 Problem Statement

The performance of the folded plate girder needs to be tested to determine behavior in two main aspects of a bridges life. First, the beam must be able to handle construction loads, and then the beam must be able to handle the loading it will experience over the life of the bridge.

A testing program has been developed for testing of the Folded plate girder. Table 1-1 summarizes the specimens tested to this date. Table 1-2 summarizes the tests that have been performed. This report focuses on the constructability testing of Specimens A and B, which are the objects of Test A1 and B1 outlined in the table. Folded plate girders were designed to be composite girders for the service life of the bridge. During construction, the girders will not be composite, so it is important that the girders can handle the construction loads. Tests were performed on two non-composite folded plate girders to determine how the girders will perform during construction.

Table 1-1 Summary of test specimen geometry

		Height	Width	Top Flange	Bottom Flange	Thickness	Side Length	Opening	Trap Height	Trap width	Ridge Height	Angle	Bend Radius	Yield Stress
	Units	in	in	in	in	in	in	in	in	in	in	degree	in	ksi
	Label	A	B	C	D	E	F	G	H	J	K	L	R	
Specimen	A	24.75	45.47	30	10	0.375	20.7	20.72	24.38	46.42	0*	75	2	65
	B	24.75	45.47	30	10	0.375	20.7	20.72	24.38	46.42	0*	75	2	65
	C	24.75	45.47	30	10	0.375	20.7	20.72	24.38	46.42	0*	75	2	65
	D	25.88	43.85	28.78	11.8	0.375	21.87	16.50	24.50	44.50	1.0	75	1.5	50
	E	25.88	43.85	28.78	11.8	0.375	21.87	16.50	24.50	44.50	1.0	75	1.5	50

* No ridge in top flange

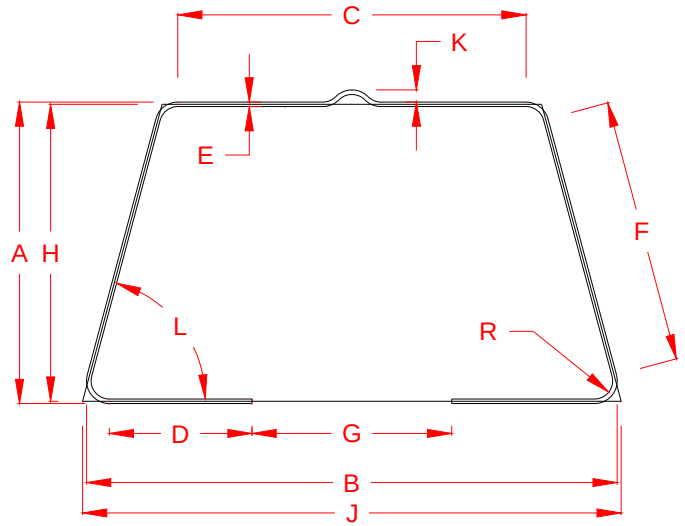

Figure 1-1 Folded plate girder cross section

Table 1-2 Summary of testing program

Tests						
ID	**Specimen**	**Length***	**Type**	**Stiffener @ load point**	**Deck**	**Comments**
A1	A	41’	Constructability	No	No	
B1	B	41’	Constructability	Yes	No	
C1	C	41’	Fatigue	No	Yes	
C2	C	41’	Ultimate	No	Yes	
D1	D	46’	Constructability	Yes	No	
E1	E	46’	Ultimate	No	Yes	Galv.
E2	E	22’	Shear	No	Yes	Galv.
E3	E	22’	Shear	No	No	Galv.
E4	E	22’	Shear	Yes	No	Galv.

* Length specifies the span length from centerline of support to centerline of support

1.2 Research Objective

The objective of this investigation is to test the performance of the newly developed folded plate girder when loaded in a non-composite situation. The investigation will include both overall girder performance as well as performance of individual components that comprise the girder.

1.3 Content

The following report contains the results and analysis of constructability testing of two folded plate girders tested as non-composite beams. The specimen descriptions, test setup, procedures, testing results, analysis, and conclusions are covered in the following sections.

Chapter

2 Test Specimens and Procedures

The following sections will provide a description of test specimens and the testing procedures. The description of the test specimens will include fabrication, section geometry, test setup, and instrumentation. The description of the test procedures will outline the test progression and explain differences between the testing of the two specimens. Nomenclature for testing includes the specimen ID and the test index. Test A1 is the first test on Specimen A. Test B1 is the first test of Specimen B.

2.1 Test Specimens

The folded plate girder resembles an inverted steel box girder, where the girder is cold bent instead of welded. There are aspects of the folded plate girder that are unique compared to box girders. First, they are folded from a single plate of steel instead of

being built up from welded plates. Second, the open bottom of the folded plate girder simplifies inspection, eliminating the in-box inspection that exists for box girders. Third, the folded plate girder cannot be cambered as easily as tub girders because of how they are fabricated, this is one of the controlling factors on maximum girder length. Another controlling factor for girder length is the length of the press brake that is used to bend the steel plates into girders.

The girder is fabricated from a single plate of Grade 65 steel. Figure 2-1 shows the fabrication steps that are determined by the geometry of the press in relation to the geometry of the girder plate.

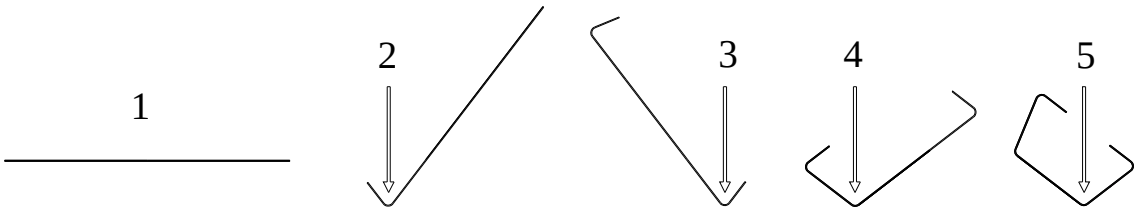

Figure 2-1 Plate folding process

The fabrication of the girder begins with a flat plate, step 1. What will become the bottom flanges are folded in steps 2 and 3. In steps 4 and 5, the corners between the top flange and the webs are formed. Figure 2-2 shows the final shape and geometry of the girder cross section.

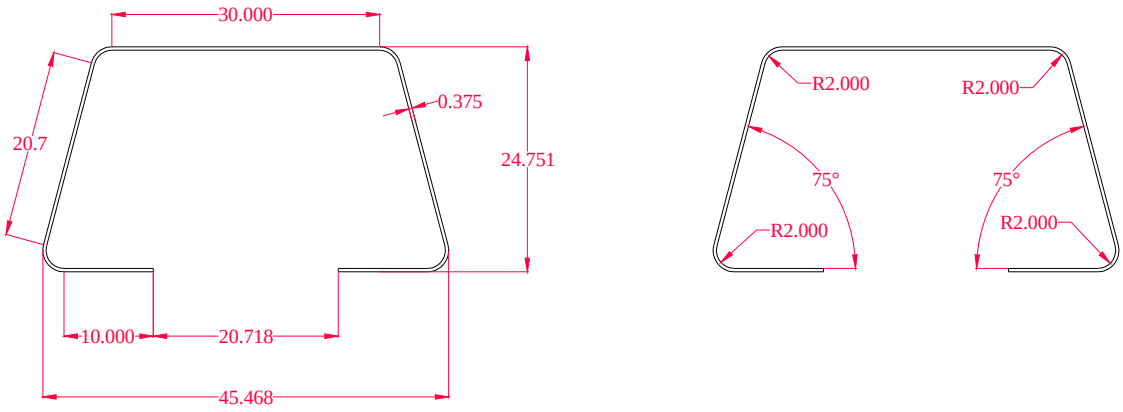

Figure 2-2 Folded plate geometry

Bearing stiffeners and plates are welded to the girders, after the basic girder shape is formed, at what will be the centerline of support for the girder ends. Figure 2-3 shows the details of the bearing plates and stiffeners.

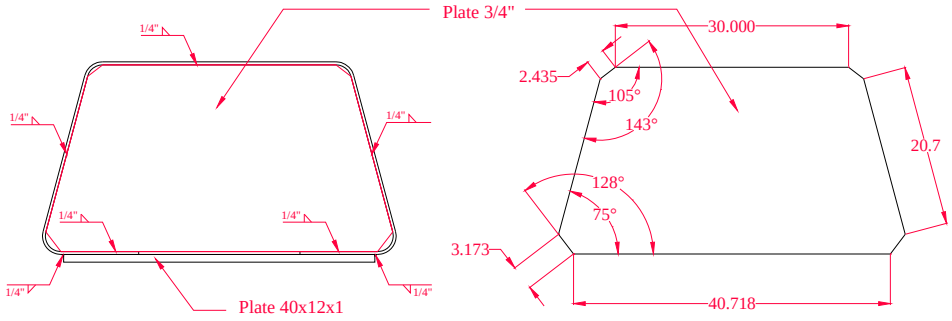

Figure 2-3 Girder bearing plate and stiffener dimensions

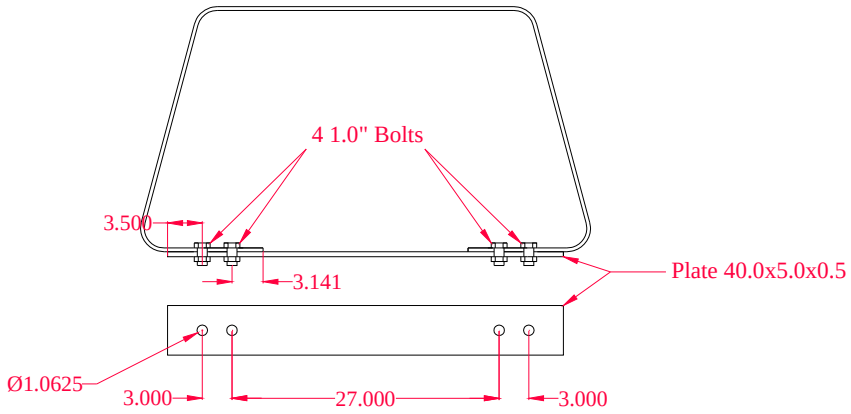

Figure 2-4 Tie plate details

Tie plates that connect the bottom flanges are then bolted to the bottom flanges. Figure 2-4 shows the tie plate details. Figure 2-5 shows the girder dimension and the locations of tie plates, bearing plates, and bearing stiffeners.

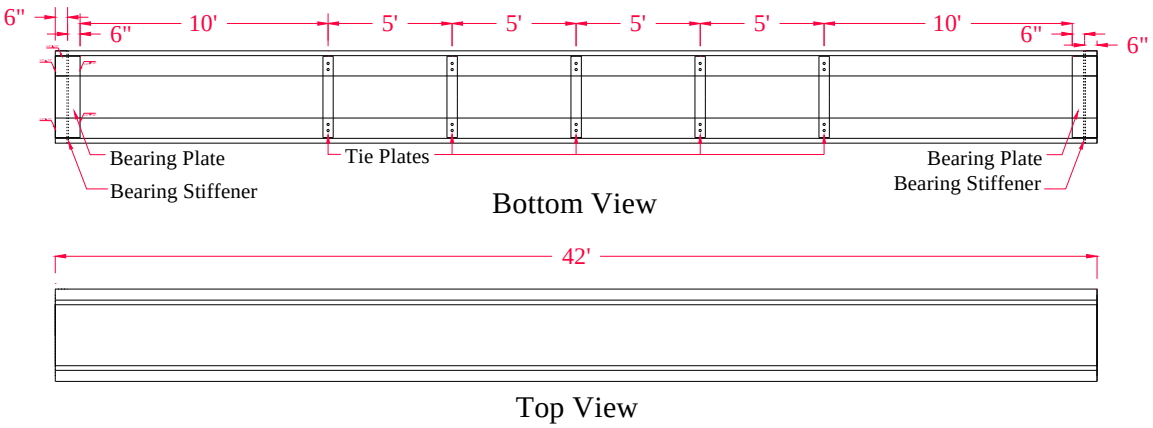

Figure 2-5 Girder dimensions

Two similar folded plate girders were tested. The girders are 42 ft long and tested over a span of 41 ft. The Girders were fabricated using 42’ x 108” x 3/8” grade 65 weathering steel plate. The plate was folded as described in the previous section resulting in a girder that is 24.75” tall.

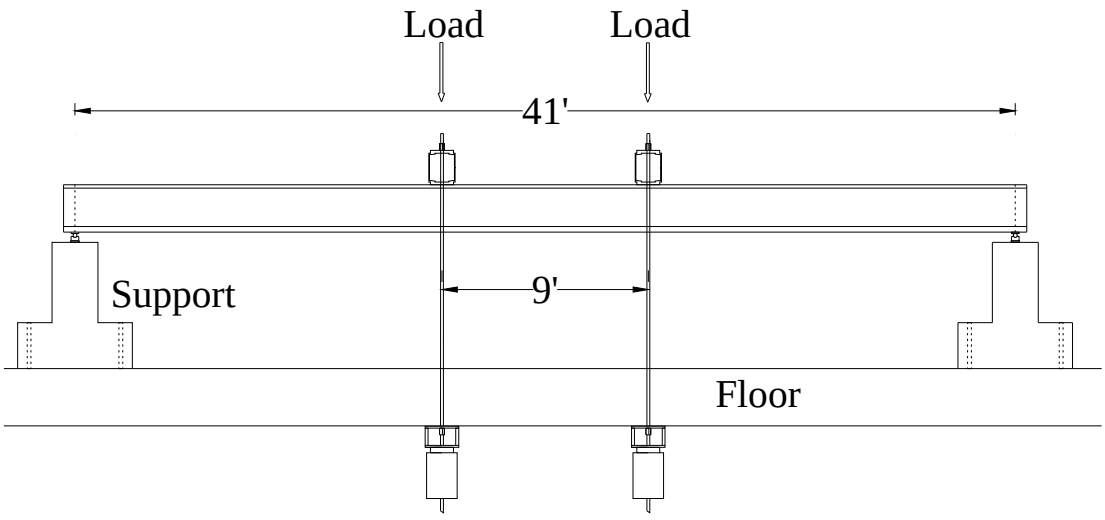

Figure 2-6 Test setup

2.2 Test Setup

Both girders were set up to be tested over a simple span of 41ft. The supports were made from reinforced concrete, which was post tensioned to the floor to eliminate any movement of the supports during testing. The girder set on rockers located directly beneath the bearing stiffener of the girder to allow for rotation of the girder during testing as can be seen in Figure 2-7. The rockers set on two layers of Teflon to allow for any horizontal movement during loading.

Figure 2-7 Girder bearing system

Load was applied using spreader beams with Threaded rods that passed through the floor and into the basement as can be seen in Figure 2-8. Bearing pads were placed between the spreader beams and the top of the girder. In the basement, there were hydraulic cylinders on each bar that created the downward loading during testing. Bracing was added between spreaders to stabilize the load setup during assembly.

Figure 2-8 Test A1 setup

2.3 Instrumentation

A variety of instrumentation was used to measure the loading, deflection, and local deformations of the beam during testing. Strain in flanges, webs, bent corners, and tie plates were areas of interest during testing. Other monitored values were overall deflection of the beam under loading and deflection of bottom flanges relative to each other.

A MEGADAC data acquisition system from Optim Electronics was also used for the experiments. Its purpose was to monitor sensors installed on the girder. Strain gages, pressure cells, and wire potentiometer based linear displacement transducers (pots) are wired directly to the Optim Electronics MEGADAC data logger. The data logger is

connected to a computer that has TCS for Windows Program software. The software allows the user to specify different sensor types, a common sample interval, and immediate download to the onsite computer.

Loading was monitored by measuring the pressure in the cylinders using pressure cells that measured the hydraulic advance and return pressures at each cylinder in the basement. Girder deflections and bottom flange separations were measured with pots at the locations shown in Figure 2-9. Pots 1-8 ran between the girder bottom flanges to monitor separation of the flanges. Pots 9-13 were located between the floor of the lab and the bottom of the girder to measure deflections.

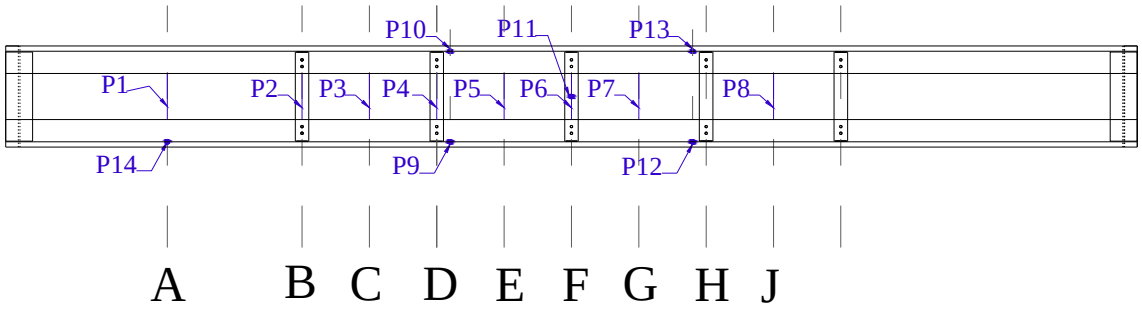

Figure 2-9 Section and pot location labels

Linear strain gages and rosette strain gages were the two types of bondable foil strain gages used to measure strains in the steel for the two tests. Linear gages were put parallel to main strain directions. Linear strain gages were used on the flanges and the webs of the girders. Rosettes are designed for determining principle stresses and strains. They have three grids oriented at 0°, 45°, and 90°. Rosette strain gages were

used on the corner bend between the bottom flange and the web. The strain gage locations for A1 can be seen in Figure 2-10.

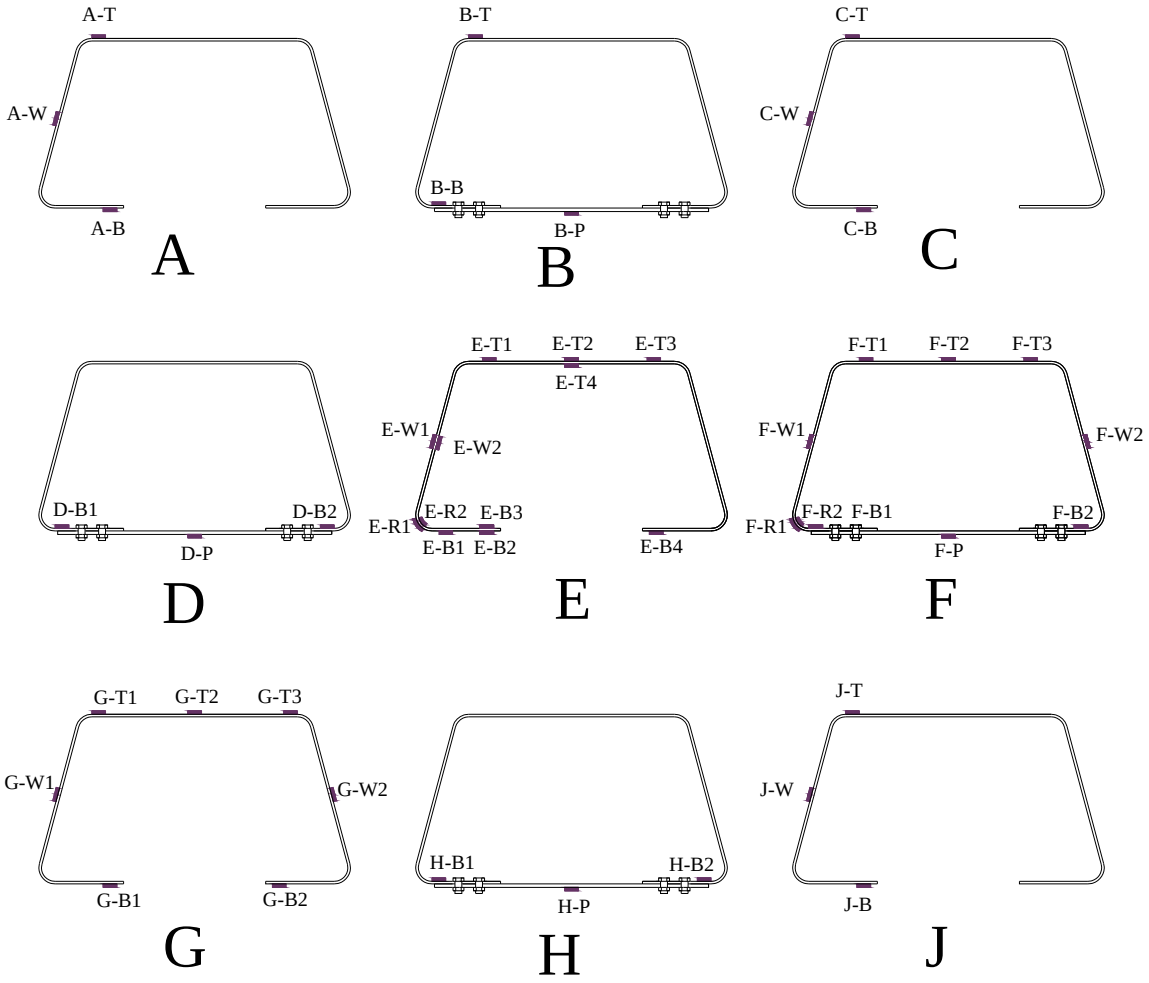

Figure 2-10 Test A1 Strain gage labels by section

The large lettering below each girder cross section designates the section along the length of the girder. Figure 2-9shows the section labels along the length of the girder. The small labels in Figure 2-10 are the gage names, e.g. F-T1 is the gage located at section F on the top flange.

Test A1 used more gauging to provide a complete picture of the girder behavior during loading. Figure 2-11 shows the gauging for Test B1.

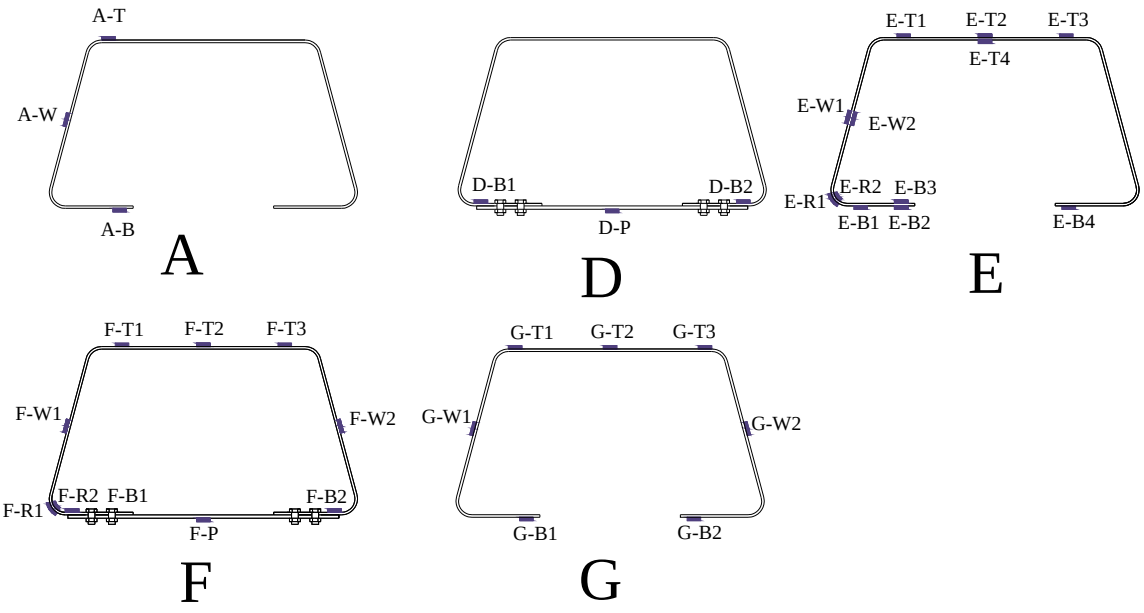

Figure 2-11 Test B1 strain gage labels by section

2.4 Test Procedures

The goal of the tests was to observe how the girders would behave in a non-composite situation such as that experienced during construction. Since the continuous loading of a wet concrete slab was unable to be simulated, the system was tested using two discrete load points. The use of two load points provides a constant moment between the load points. The location of the load points was selected to encompass the area of greatest interest. Two symmetric load points were located 4.5 feet from the span centerline as can be seen in Figure 2-12.

Figure 2-12 Load points

The folded plate girders were loaded in flexure after the experiment was set up and the testing equipment was wired and running. Test A1 and Test B1 used the same loading configuration. Load was applied to the girders up to failure.

Test A1 had two phases. The objective of the first phase was to examine the effectiveness of the tie plates. The objective of the second phase was to test the girder when loaded to failure.

During the first phase, the girder was loaded three times at low load ranges where girder behavior was both linear and elastic. First, the girder was loaded with all tie plates in place and then unloaded. The middle three tie plates at sections D, F, and H were removed for the second loading. After the girder was unloaded again, the tie plates were re-installed and it was loaded again.

Specimen A was loaded to failure during the second phase of loading. During ultimate loading, the middle three tie plates were not connected. The tie plates were disconnected by removing the bolts at one end of the tie plates as can be seen in Figure 2-13. The Specimen A was tested without stiffener plates at the loading points. The second specimen, Specimen B, had the stiffener plates added at the load points to reduce the local deformation behavior due to stress concentrations caused by the concentrated loads. During Test B1, all tie plates remain installed throughout testing. Specimen B was loaded to failure.

Figure 2-13 Disconnected tie plate at section H

Shear studs can be seen on the top flange of Specimen B in Figure 2-14. Specimen A did not have shear studs on the top flange. Originally, Specimen B was going to be used for a composite test. After the first test, it was desired to do a second non-composite test. Specimen B was available and was selected. The shear studs were removed from the load points so that loading would not be affected. The presence or absence of shear studs had no effect on the performance of the girders.

Figure 2-14 Test B1 setup

Chapter 3

Test Results and Discussion

This chapter provides a presentation of the experimental data and observations from Test A1 and Test B1. Behavior at construction load levels and failure mechanisms will be the focus of testing. Material properties are covered in the first section. The following sections will present the results from the two tests.

3.1 Steel Properties

Tensile tests were performed on samples from both girders after testing had been completed. Samples were cut from the web of the girder, near the end of the beam, where stains remained well within the elastic limit during testing. Samples were cut in two directions; samples that ran parallel to the length of the girder or longitudinal and samples that ran perpendicular to the length of the girder or transverse.

Samples were tested according to ASTM A370. Samples were testing using a MTS hydraulic load frame. The computer program that runs the load frame allows the user to program the loading sequence and desired strain rates. The load frame force and displacement are recorded directly from the load frame sensors to the control program. An extensometer is attached to each steel tensile specimen after it is secured in the load frame. The extensometer measures the strain at the desired section of the sample.

Strain rate affects the results of tension testing of steel; test data can be shifted more than 20% if care is not exercised in conducting the tension test(Galambos, 1976). ASTM specifies strain rate limits used for steel tensile tests.

Testing begins with a constant stain rate during the elastic portion of the tensile test. After yielding begins, there is a procedure, outlined by the SSRC, for obtaining the static tensile yield strength. When the strain reaches approximately 0.2% offset the test should be interrupted by holding a constant strain or stopping the cross head motion. The load frame motion is paused and held at a constant displacement until the load is stabilized. After the load stabilizes the strain rate can be resumed. This procedure of strain holding should be performed two more times in the yield region. The results of this process of determining static yield strength can be seen in Figure 3-1 as the three dips in the yield region. The static yield stress is recorded as the low values at each of the interruptions. The three values are then averaged. After strain hardening begins the strain rate was increased according to ASTM procedures until failure occurs. This is to reduce the amount of time each test requires.

Table 3-1 Folded plate girder tensile test results

Test/Direction	Yield Stress (ksi)	Ultimate Stress (ksi)
A1/ Longitudinal	73.5	89.5
A1/ Transverse	73.5	89.1
B1/ Longitudinal	71.9	88.4
B1/ Transverse	73.7	89.9

Groups of four samples were tested in both directions for each girder, resulting in 16 samples tested. The results from each group of four were averaged and can be seen in Table 3-1 Folded plate girder tensile test results. Figure 3-1 shows a typical stress strain graph that resulted from the tensile tests. This specific graph is from a sample that was from the first girder tested and oriented in the longitudinal direction. Recall that the steel specified was Grade 65W.

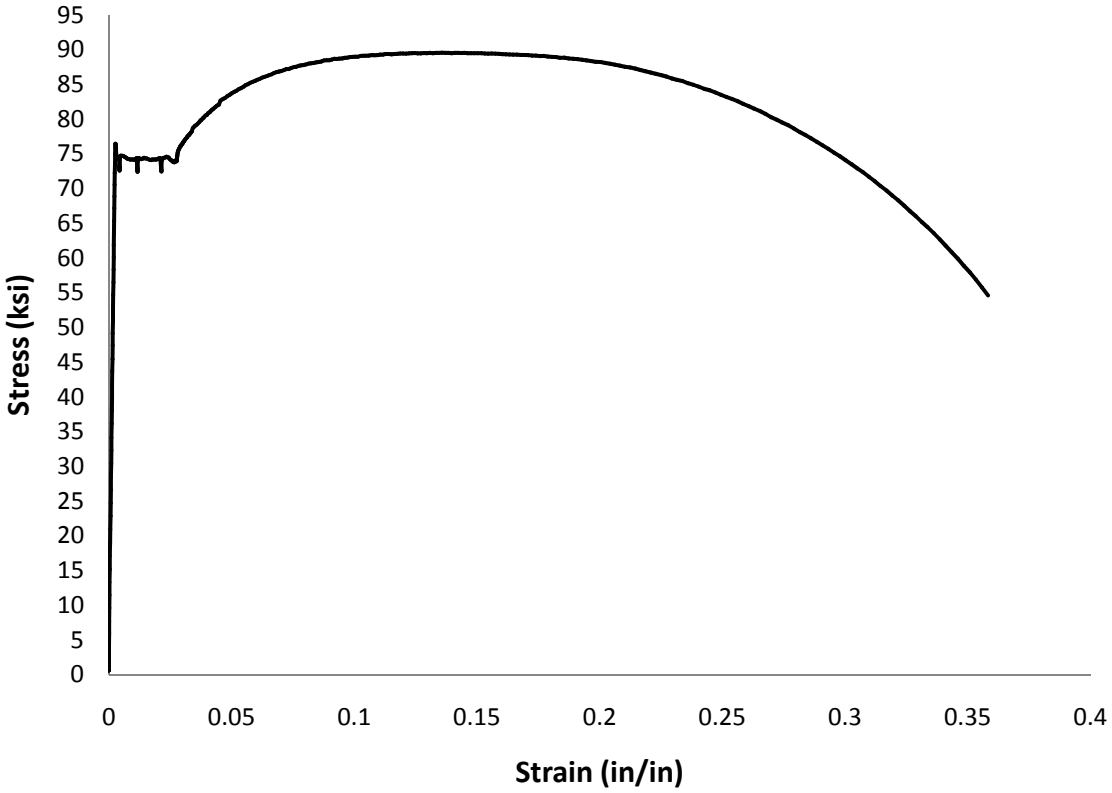

Figure 3-1 Steel Stress-Stain plot from Test A1

3.2 Test A1 Results

The first girder was tested following the procedures described in the previous chapter. Specimen A was tested without stiffener plates at the loading points. This section will examine the results from the testing. The overall performance of the girder and the performance of specific components of the girder including the performance of the tie plates and the affect they have on girder behavior will be discussed. Strain distributions throughout the girder will also be examined.

Figure 3-2 shows the moment deflection graph for Test A1. The graph contains data from the vertical pot, P11, located at midspan. The orange line represents the maximum amount of moment that would be experienced during construction.

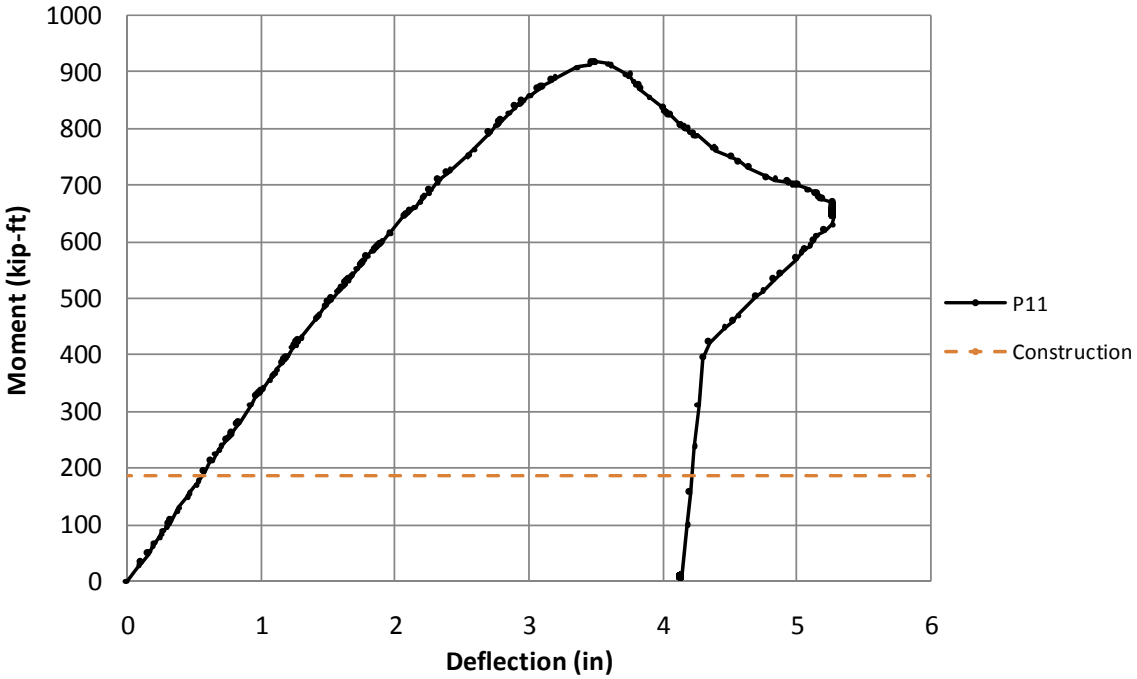

Figure 3-2 Moment-deflection curve of Test A1

The girder deflects linearly up past the construction moment and up to roughly 2 times the construction moment. After this, the graph slowly starts to depart from the linear and curve ever so slightly. This is when the concentrated loading reached levels to begin buckling the top flange as can be seen in Figure 3-7. As the load increased the deformation of the top flange increased which in turn reduced the ability of the girder to resist flexure, which is reflected in the data. The top flange buckling increased up to the ultimate loading when the web also began to buckle. The girder could no longer take any additional load and load began to decrease as deflection continued to increase. The beam was loaded up to 5.3 in of deflection at which point the girder was unloaded and testing was concluded.

Figure 3-4 shows all vertical pot data from the moment deflection graph for the ultimate test. The curves in the graph are from pots that were located at the load points and at mid-span. Recall from Figure 2-9 the location of the pots. P9 and P10 were at the west load point on each flange and P12 and P13 were located at the east load section on either flange. The deflections of the four pots located at the load points all match, as they should, because they are all located symmetrically about the center of the span. The pot at mid-span, P11, has a slightly higher deflection as expected.

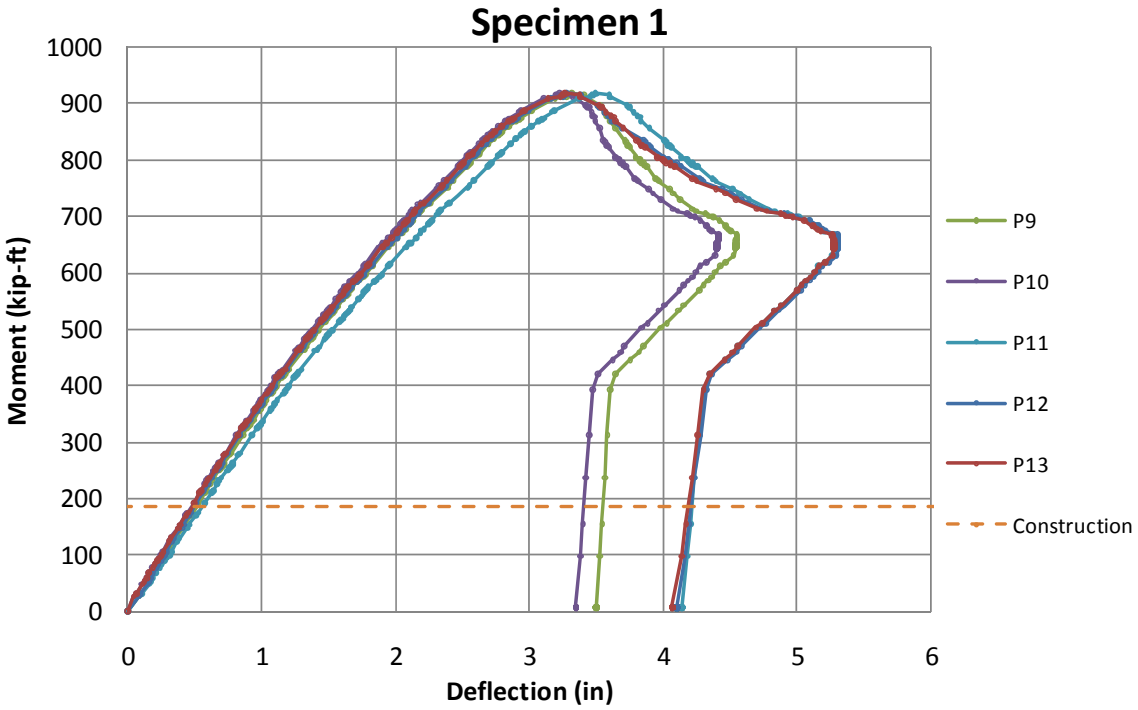

Figure 3-3 Moment-deflection plot of Test A1

Figure 3-4 through Figure 3-9 show the girder before and after the top flange and web buckle. Figure 3-10 shows the buckling of the top flange and webfrom inside the girder.

Figure 3-4 Specimen A before testing

Figure 3-5 Specimen A during testing

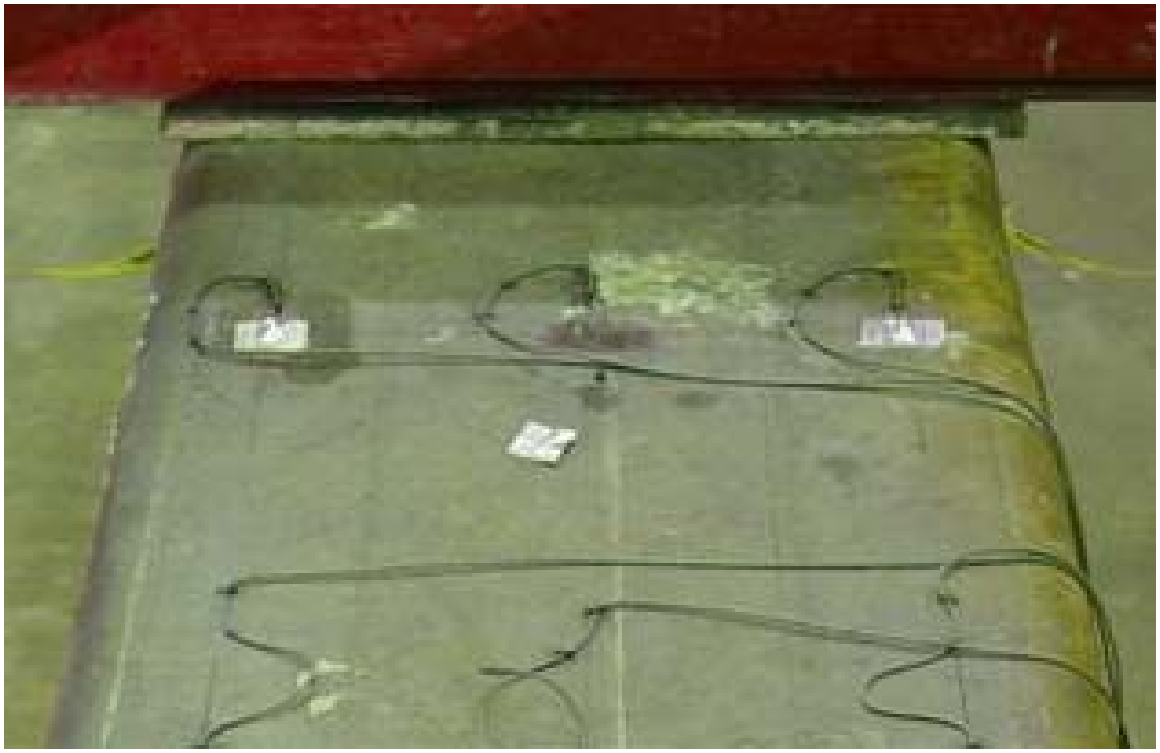

Figure 3-6 Top flange before loading

Figure 3-7 Top flange during loading

Figure 3-8 Girder web before loading

Figure 3-9 Web deformation from loading.

Figure 3-10 Inside of folded plate girder after failure

Figure 3-11 shows the north side of the girder after loading with the close spreader beam being the west load point. These two figures do a good job of showing the web buckling and the fact the girder has buckled under the east load point more than the west load point. This can also be seen in the moment deflection graph, Figure 3-2, and is the reason that the pots P12 and P13 show higher deflections than P9 and P10 after the peak load.

Figure 3-11 North side of girder facing east showing girder deflection and web buckling

Figure 3-12 North side of girder facing east showing girder deflection and web buckling

One of the goals of testing was to test the effect of the tie plates that connect the bottom flanges. The tie plates are key components to maintaining the girder shape during loading by resisting separation and rotation of the bottom flanges. A series of loading sequences were carried out to examine the performance and affect of the tie plates.

Initially the beam was loaded with low loads relative to the ultimate capacity of the girder. The first loading was performed with all of the tie plates in place. The specimen was loaded to a moment of 210 kip-ft, and can be seen in Figure 3-13 as the red line. The graph is showing the data from the pot P7 located at the tie plate at mid-span of the girder. Linear elastic behavior can be seen. The flange movement was very small. The specimen was unloaded, tie plates at D, F, and H were removed, and the specimen was loaded to 270 kip-feet. The Figure shows the second loading with a purple line.

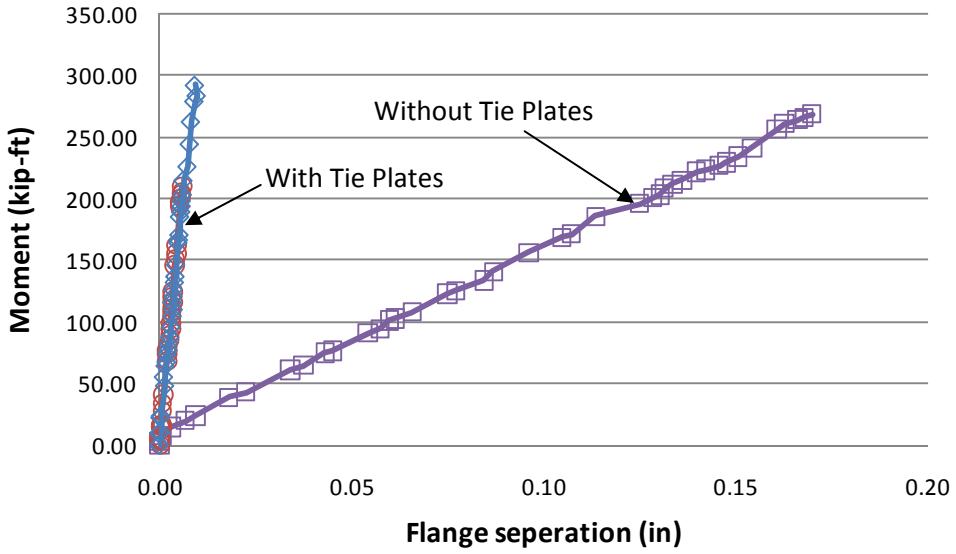

Figure 3-13 Moment-displacement plot from Pot P7 during phase 1 loading

The slope of this line is different, resulting in much greater flange separation with the same loading. The girder was then unloaded. The tie plates were bolted back in place and the specimen was loaded again to 294 kip-ft. The blue line in Figure 3-13shows this final loading. After re-installing the tie plates, the girder regains the same stiffness that was displayed by the first loading with the tie plates installed.

Figure 3-14 shows the girder deflection from the vertical pot P10 for the same three loading sequences. Unlike the flange separation, the girder deflection is not affected by the tie plate's presence at these load levels.

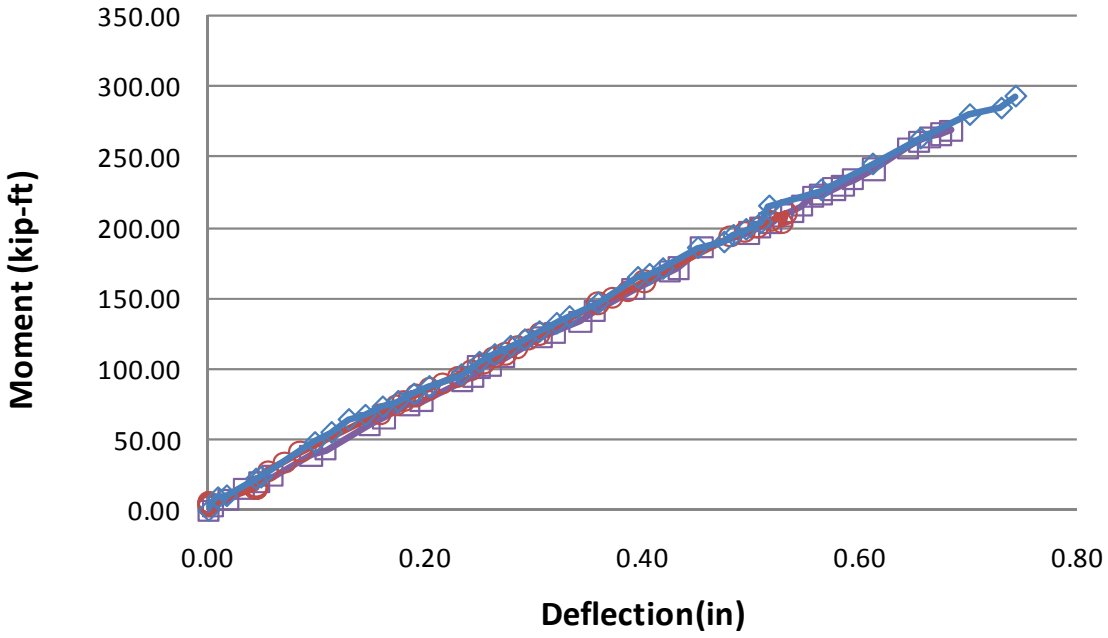

Figure 3-14 Moment-displacement plot from pot P10 during phase 1 loading

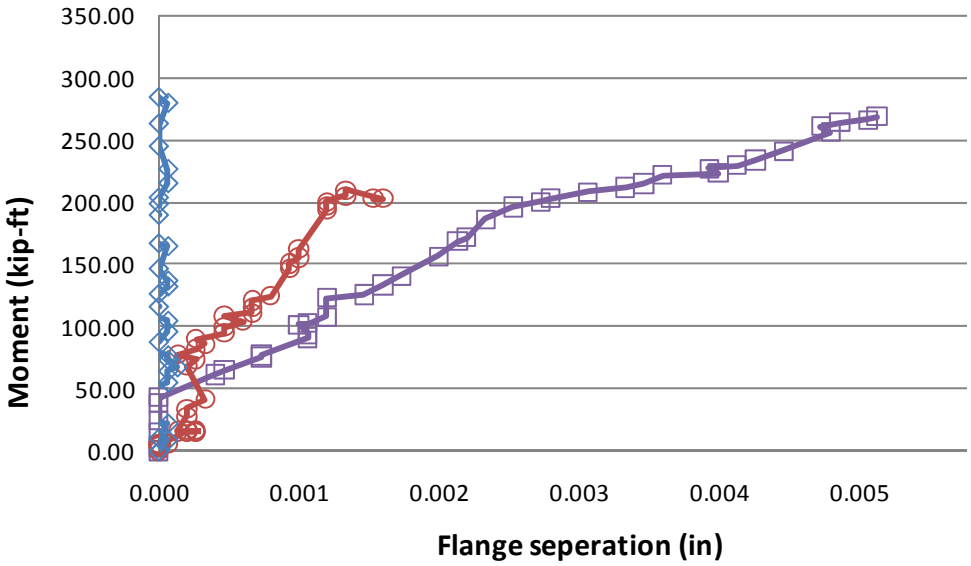

Figure 3-15 Moment-displacement plot from pot P2 during phase 1 loading

Of the five tie plates, the ones that were removed were the three inside plates. The two exterior plates located 10 feet from each support remained throughout testing. Pot P2 is located at the west tie plate. Note in Figure 3-15 that the greatest movement, regardless of the number of tie plates, was less than one hundredth of an inch, which should be expected at a tie plate location.

Figure 3-16 isa comparison of all horizontal pot data, at a load of 195 kip-ft, based on the presence of tie plates. The red series is with tie plates in place. The deflections are all on the magnitude of thousandths of an inch. The blue series shows data from the same pots but the data is from loading without the three tie plates installed. The flange separation is on the magnitude of tenths of an inch. The result is that tie plates are both necessary and effective at preventing flange separation and maintaining consistent girder geometry.

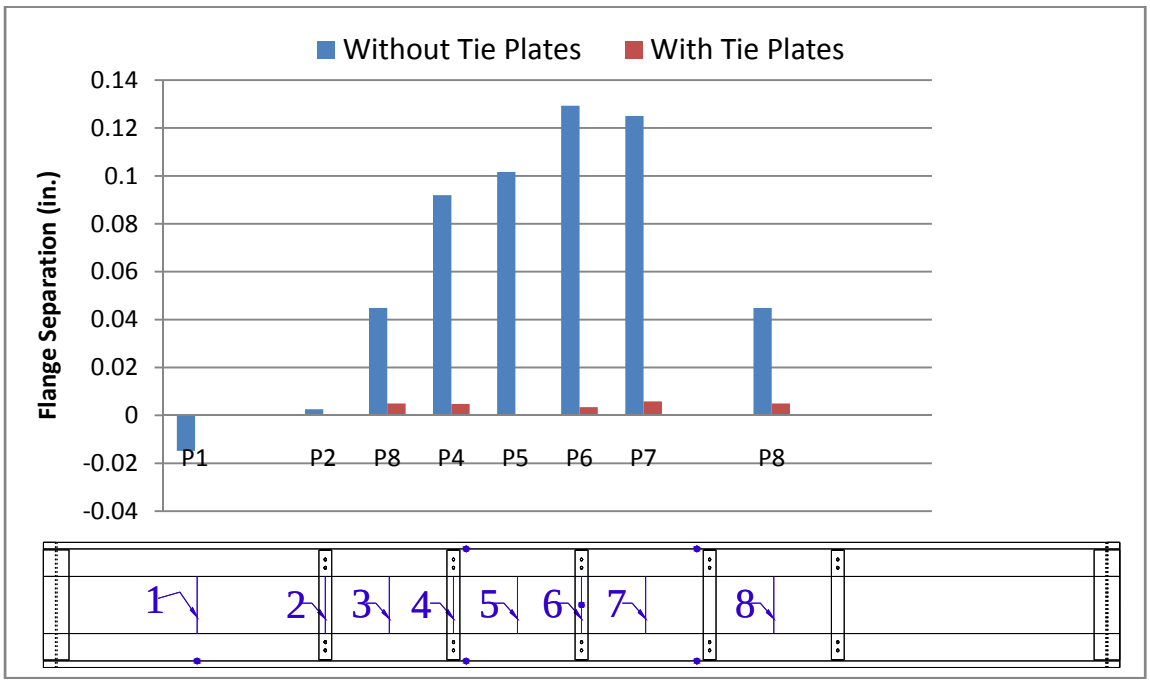

Figure 3-16 Flange separation comparison at 195 kip-ft

Following the three load sequences, the tie plates at sections D, F, and H were removed and the ultimate test was performed. Figure 3-17 shows the girder deformation after testing was concluded. The bolt holes in the bottom flange and tie plate, which were once aligned, are now offset because of bottom flange separation.

Figure 3-17 (left) Flange and tie plate bolt hole alignment after loading, (right) girder movement at support.

Strain gages were placed on the tie plates to monitor tie plate performance. The following graph of moment vs. strain, Figure 3-18, shows strains experience by the tie plates.

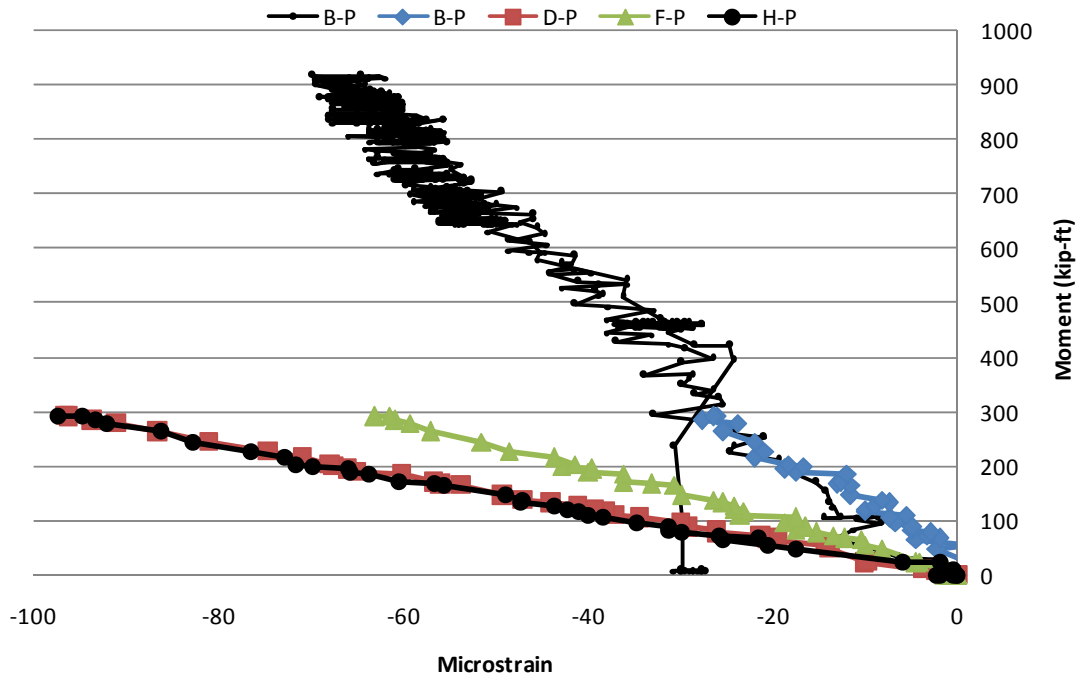

Figure 3-18 Tie plate strain data

Note the tie plate at section B was always connected; Tie plates at sections D, F, and H were connected for two loading sequences, and disconnected in between and for the ultimate loading. That is why the strain data in figure only goes to a moment of 300 kip-ft for the three gages at section D, F, and H. The graph has two series of strain data for strain gage B-P. The blue series was from the same loading sequence as the series for D-P, F-P, and H-P. The other series of data for B-P is from the ultimate loading sequence. As expected, the strains at section B were the lowest. Sections D and H, which are symmetric to the center of the bridge, have the same strains. Based on the moments

along the span, sections D and H should have the same or less strain than section F. The reason they are greater is that sections D and H are near the load points and the local deformation caused by the load points creates a greater strain on the tie plates located at these sections. Although there is not strain data for all of the tie plates up to ultimate loading, even if the strains were scaled up to the ultimate moment of 920 kip-ft, the maximum strain would only be around 300 microstrain, that is only 12% of the yield strain that was obtained from the material tests. At the construction moment of 190 kip-ft the maximum strain in any tie plate is 65 micro strain which is less than 3% of yield.

The following figures show the strain of different areas throughout the girder during the three loading sequences where the tie plates were initially in place, then removed, and finally replaced again. Each graph contains data from a single strain gage. The first, second, and third loading sequence are represented by the blue, red, and green respectively. The blue and green were the result of the tie plates being in place and the red is from the tie plates being removed. Figure 3-19 shows strain vs. moment for section C. The strains in top and bottom flanges of section C were not affected by the presence of tie plates.

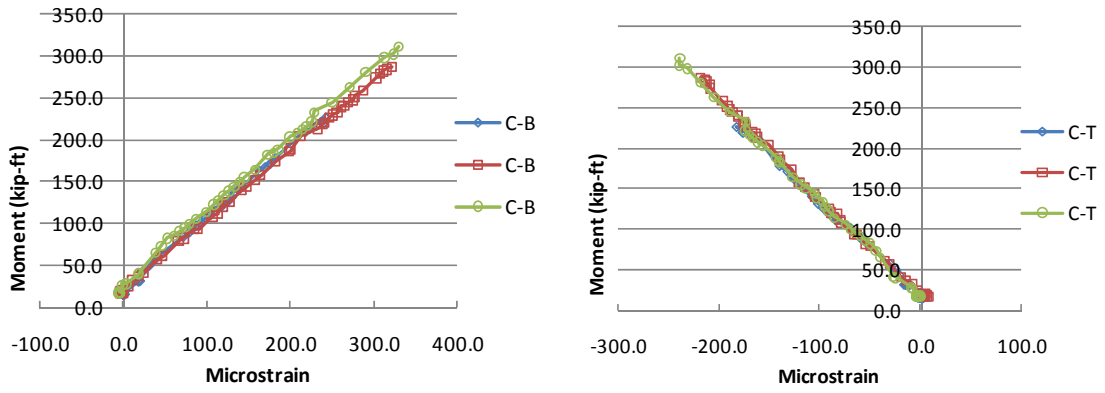

Figure 3-19 Strains at section C during three loading sequences

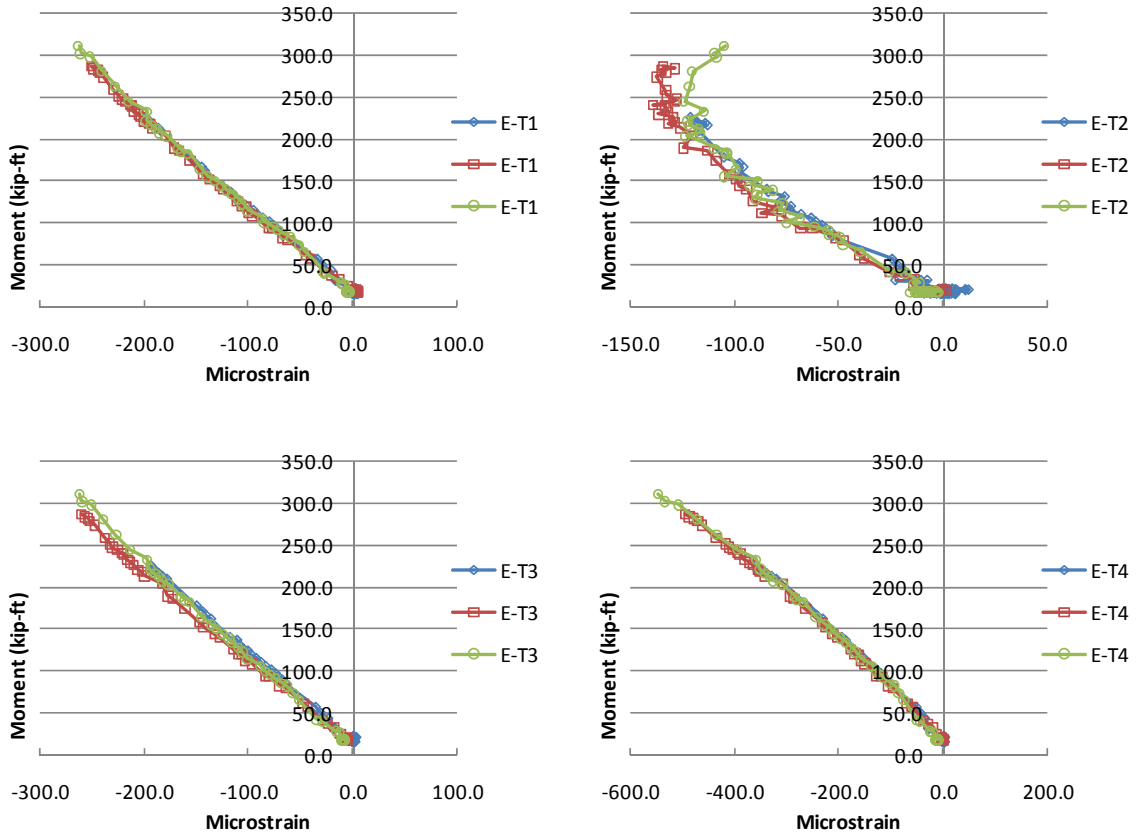

Figure 3-20 Section E top flange strains

Figure 3-20 shows the moment vs. strain curves for the top flange of section E. The strains in the top flange of section E were not affected by the presence of tie plates. It can also be seen that none of the graphs show linear behavior. This is the result of the buckling of the top flange. E-T2, which is located at center on top of the top flange, most clearly illustrates the affect of the top flange buckling. It is also important to note that the strains returned to initial levels each time the specimen was unloaded. That means that the buckling was not affecting the elastic behavior of the beam at these load levels. Note from previously that the construction moment was around 190 kip-ft.

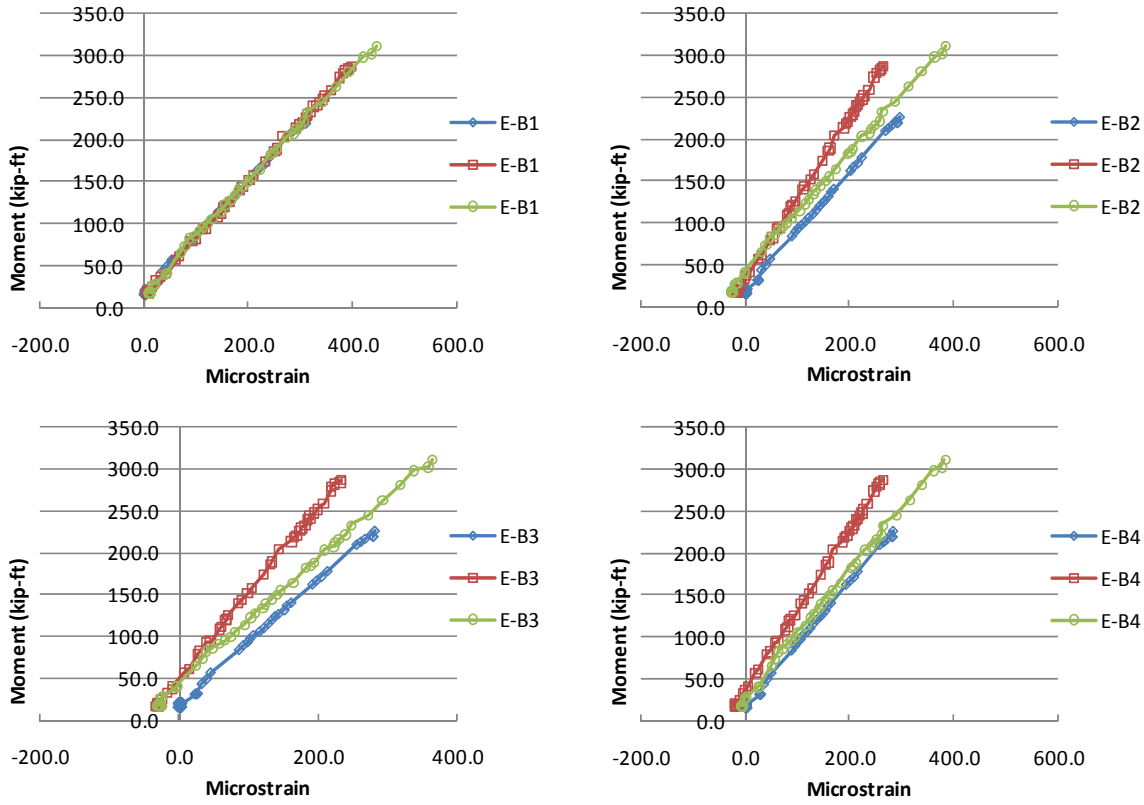

Figure 3-21 Bottom flange strains at section E

Figure 3-21 shows the strains located in the bottom flange at section E. E-B1 was located on the bottom flange near the corner where the flange and web meet. E-B2, E-B3, and E-B4 were all located closer to the free edge of the bottom flanges. E-B1 was not affected by the presence of tie plates, but the other three gages were. Without the tie plates the girder shape was not preserved. This allowed the flanges to rotate resulting in the flanges not maintaining their horizontal orientation. As soon as the flanges leave the horizontal position, the higher side will experience lower strains.

Figure 3-22 shows the strains at section F which is at mid-span of the girder. Again, there was non-linear behavior in the top flange caused by buckling but no affect on the magnitude of the strains related to the presence of tie plates.

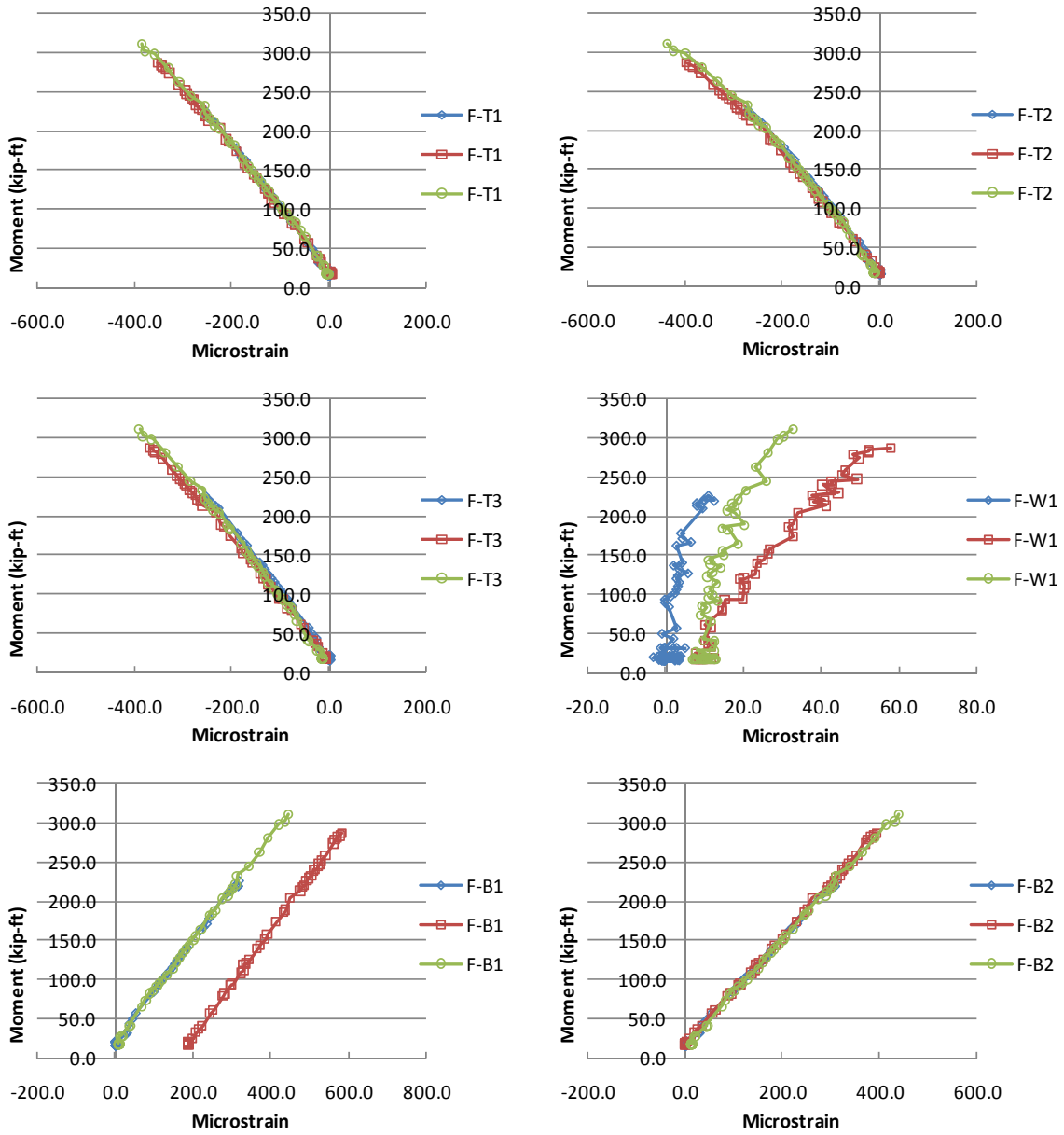

Figure 3-22 Strains at section F

The web gage and one gage on the bottom flange, F-W1 and F-B1 respectively, show the affect of tie plates while the other bottom flange gage, which is located on the other flange and is symmetric to the first, shows no affect from the tie plate removal.

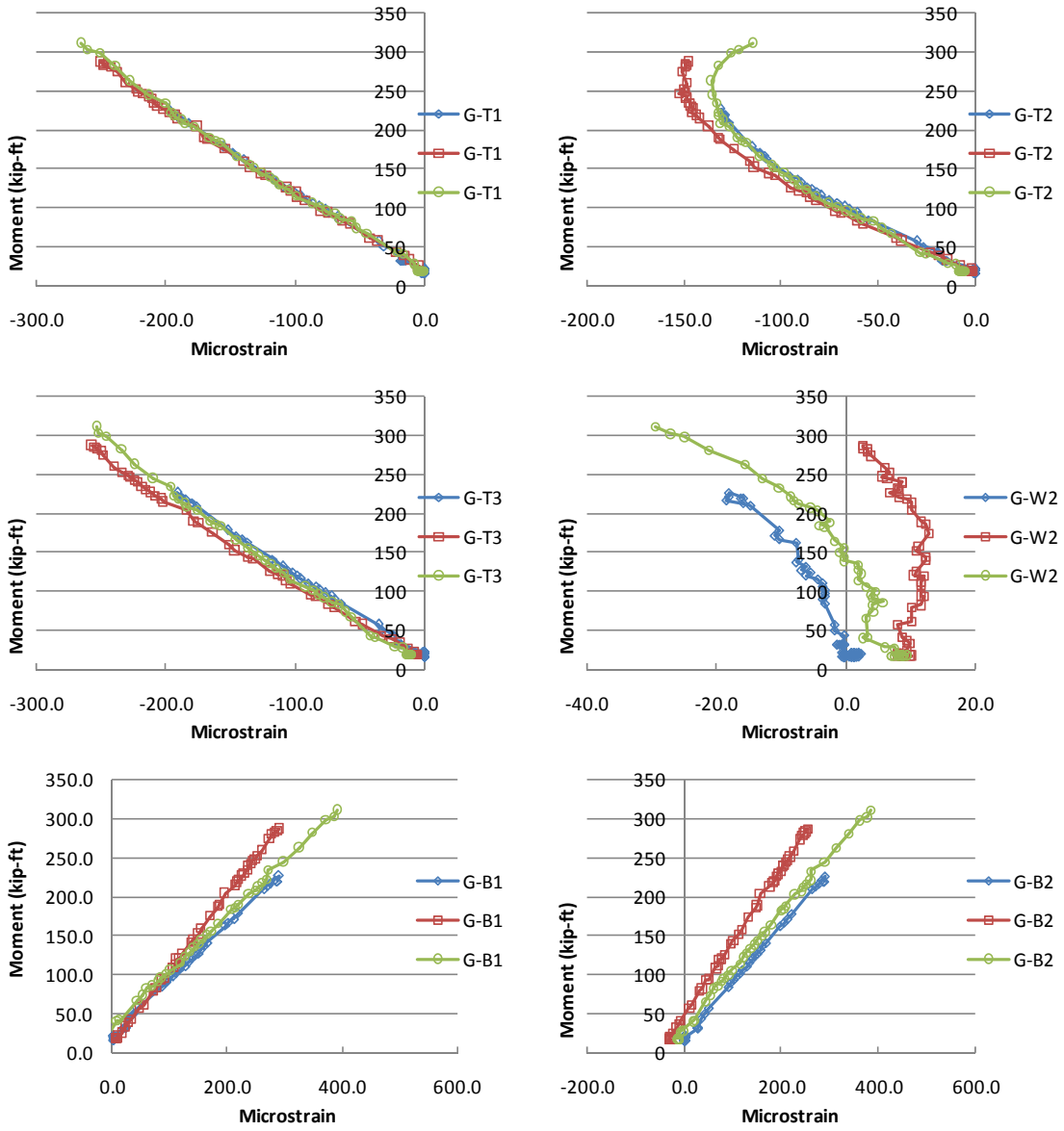

Figure 3-23 Strain at section G

Figure 3-23 shows the strains at section G. Section G shows very clearly the affect of top flange buckling. The two gages located near the webs, G-T1 and G-T3, are linear, while G-T2, which is located in the middle of the top flange, is greatly affected by the buckling of the top flange and slightly affected by the absence of tie plates.

Strain distribution in the girder provides a good way to monitor beam behavior and can reveal local deformations and failure mechanisms. Strain distribution through the height of the girder is presented with microstrain on the horizontal axis and girder elevation on the vertical axis as seen in Figure 3-24.

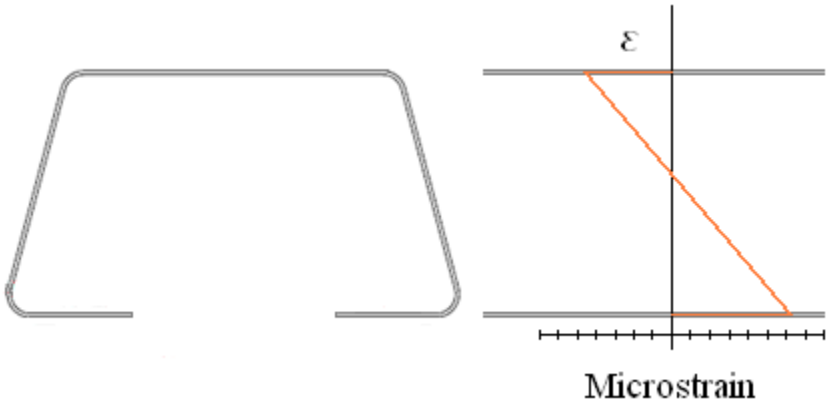

Figure 3-24 Strain distribution illustration

While strains remain linearly elastic, strain distribution can be calculated by using the Euler-Bernoulli classic formula for determining the bending stress in a beam under simple bending, equation 3-1. Hooke's Law, Equation 3-2, can then be used to convert the stress into strain.

$$\sigma = \frac{Mc}{I} \qquad \textbf{3-1}$$

Where:

σ = stress
M = moment
c = distance from neutral axis
I = moment of inertia

$$\varepsilon = \frac{\sigma}{E} \qquad \textbf{3-2}$$

Where:

ε = strain
σ = stress
E = Modulus of elasticity

The following figure shows the strain distribution of all the strain gages at section E at the construction equivalent moment of 190 kip-ft. Section E has the most comprehensive gaging configuration. There are several things of note in this figure. First, note the orange line that shows the theoretical strain distribution based on the moment at that cross section of the girder. All other points in the figure are test data strains from the gages at section E. The gage configuration can be seen in Figure 2-10.

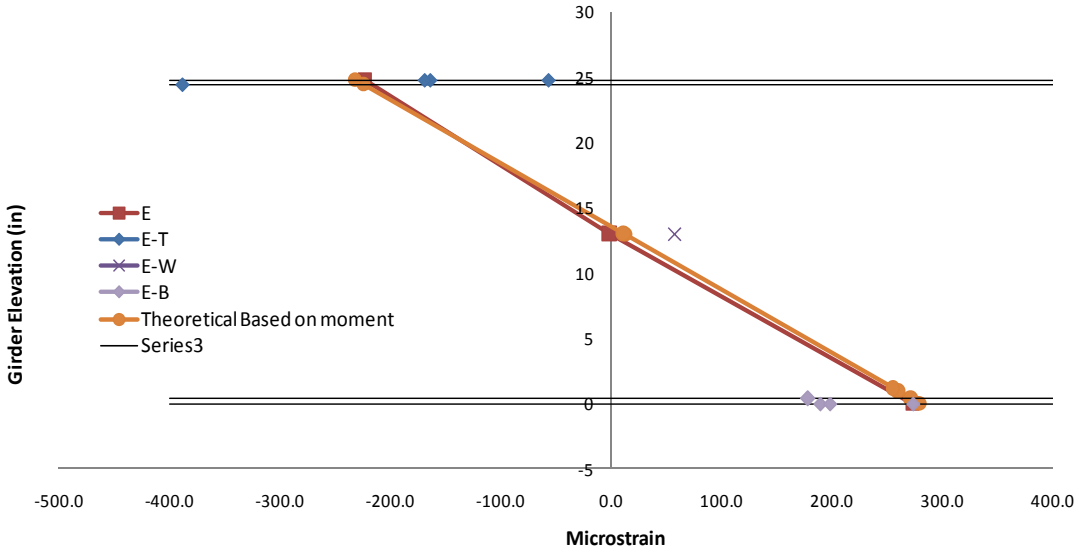

Figure 3-25 Strain distribution at section E at construction moment

There are data points that do not match the theoretical strain distribution. The strains in the top flanges were affected by the local deformation and buckling caused by a combination of the concentrated loading and the wide top flange. The two points nearest to the theoretical point are from gages E-T1 and E-T3. The top flange at these points was near the webs, which braced/stiffened the top flange to resist buckling. The two farthest points in the graph are E-T2 and E-T4, which were located at the center of the top flange with one located on the top of the flange and one located on the bottom of the flange. The location of the gages with respect to each other and the large difference in strains at each gage gives a strong indication of local deformation in the flange. The point in the graph that matches the theoretical strain is the average of E-T2 and E-T4. By averaging the two data points, the secondary strains from the local deformation cancel each other out and the resulting strain is the compression resulting from flexure of the beam.

Next look at the points on the strain distribution that are located at the bottom of the girder in the bottom flanges. E-B1 is the point that matches the theoretical. This gage was located on the flange near the web. The other three points were located near the free edge of the flanges. It is unclear why the strain is so much lower, but the same results were seen all along the girder. In all cases, data from bottom flange gages that were closer to the web provided data that matched well with the theoretical strain data. On the other hand, data from the gages located near the free edge of the flanges consistently had strains lower than the theoretical strains.

Figure 3-26 shows the strain distribution at section F. Once again, there is a theoretical strain distribution graphed with the strain distribution that resulted from the testing data. The two strain distributions are from the gages on each side of the girder. One distribution consists of F-T1, F-W1, and F-B1, while the other is composed of F-T3, F-W2, and F-B2.

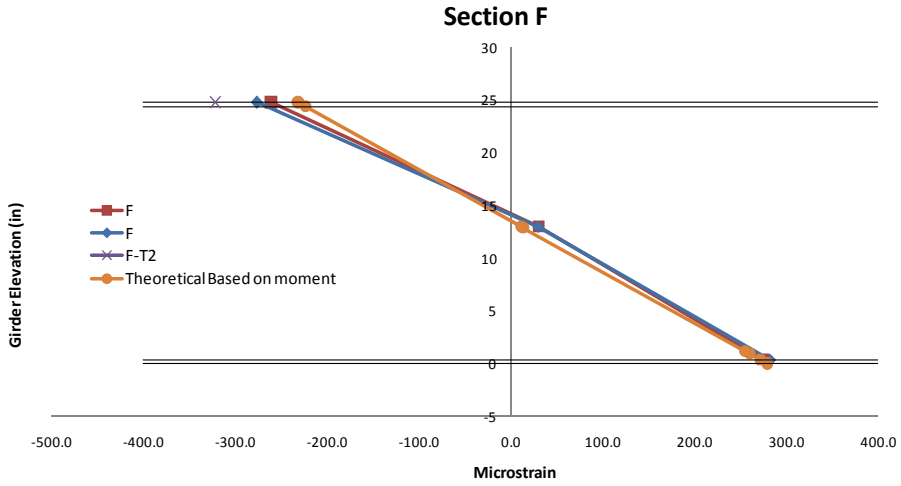

Figure 3-26 Strain distribution of section F at construction moment

The strain distributions match closely to the theoretical strain distribution. The data point that is furthest from the theoretical is F-T2, which is located at the center of the top flange. The difference is once again the result of the top flange buckling. The other top flange strains are slightly low also but to a lesser extent. This is because those gages were located near the webs. The bottom flange strains match and it is important to note once again that the location of these strain gages, F-B1 and F-B2, were on the bottom flange near the web.

The Following figures show the strain distribution at loads that are at construction loads(Figure 3-27), 2 times construction loads(Figure 3-28), Three times construction loads(Figure 3-29), and at the ultimate capacity of girder(Figure 3-30). The graphs illustrate the progression of the strain distribution and buckling as loading increases. Notice how much the web buckling is affecting the strains at the web strain gages by the time failure occurs. The web strain gages at Section E are located on both sides of the web, separated only by the thickness of the plate.

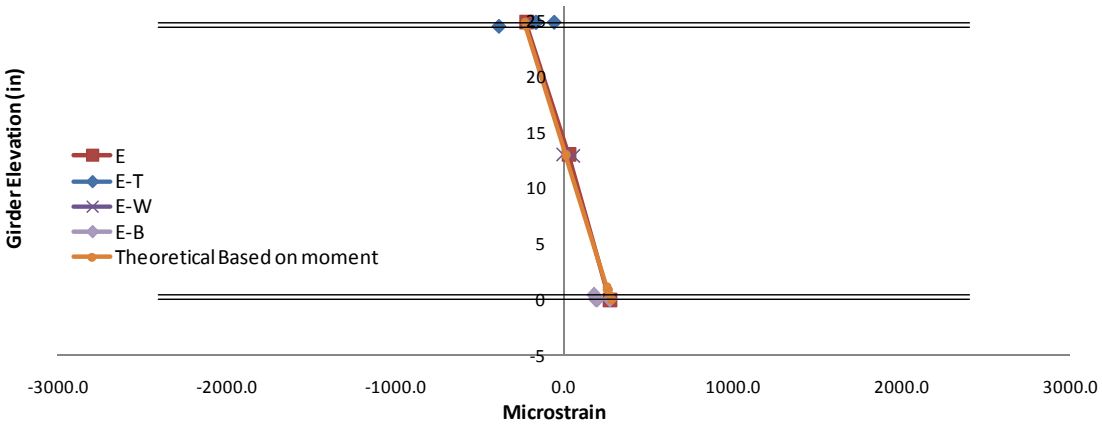

Figure 3-27 Strain distribution at construction moment

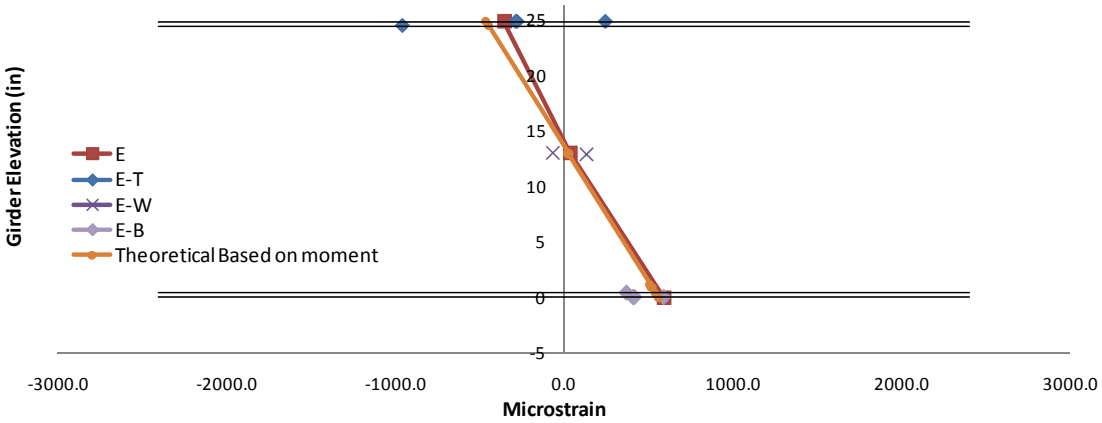

Figure 3-28 Section E strain distribution at 2 times construction moment

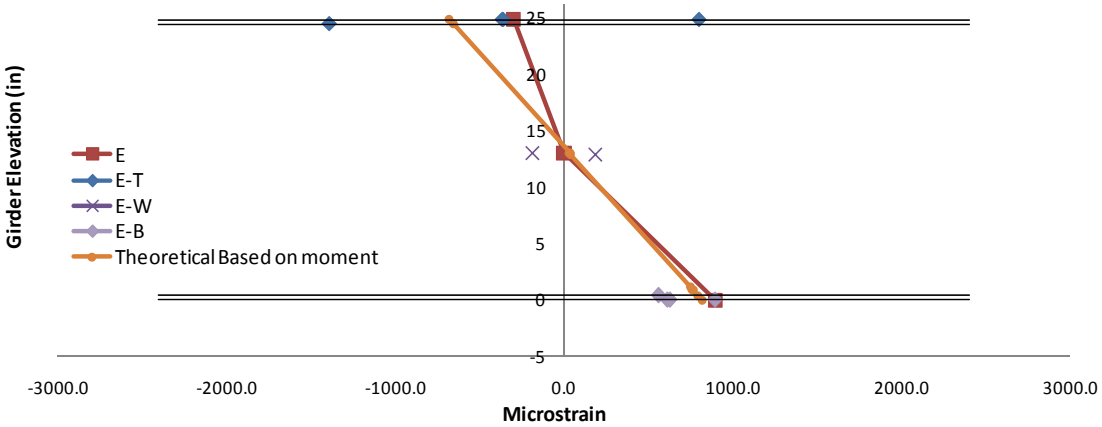

Figure 3-29 Section E strains at 3 times construction moment

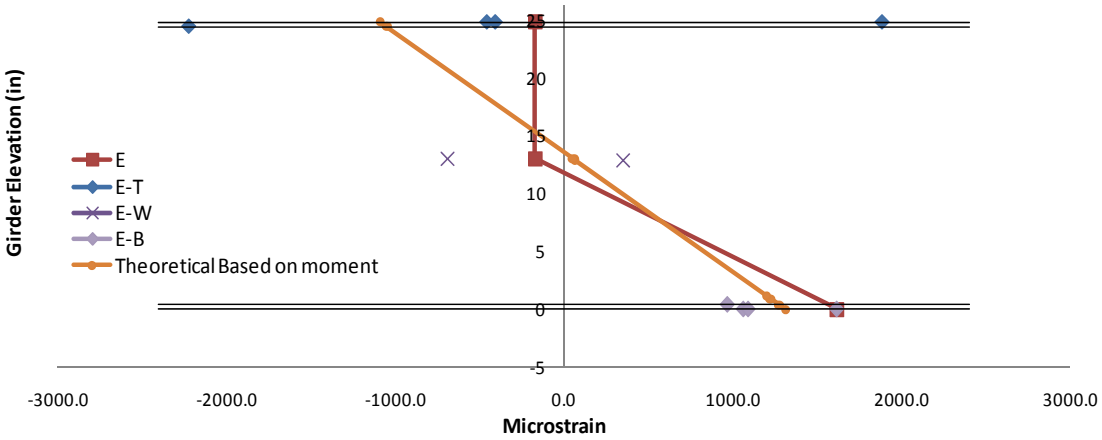

Figure 3-30 Section E strains at ultimate moment

As the load increases so does the deviation from the theoretical. This can also be seen in the following graphs of section F. The strains at Section E and F deviate from the theoretical in opposite directions. This is because at section E the top flange is buckling upwards while the top flange at section F is buckling downwards. The top flange buckled down at the load points and buckled up adjacent to them creating a cause and effect wave extending out from the load points.

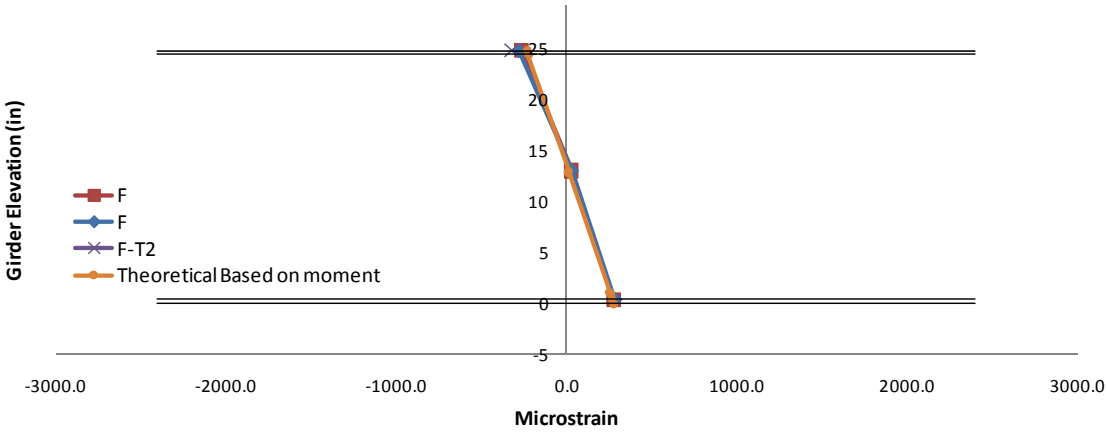

Figure 3-31 Section F strains at construction loading

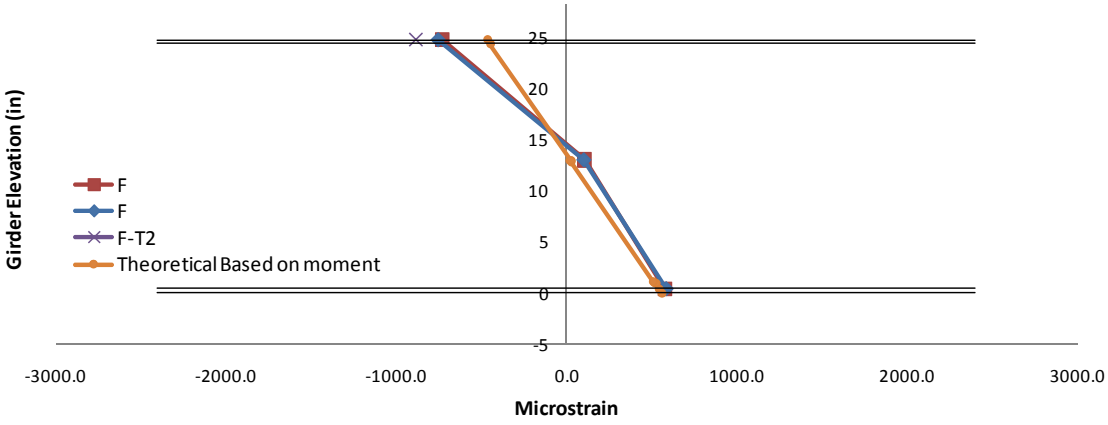

Figure 3-32 Section F strains at 2 times construction loads

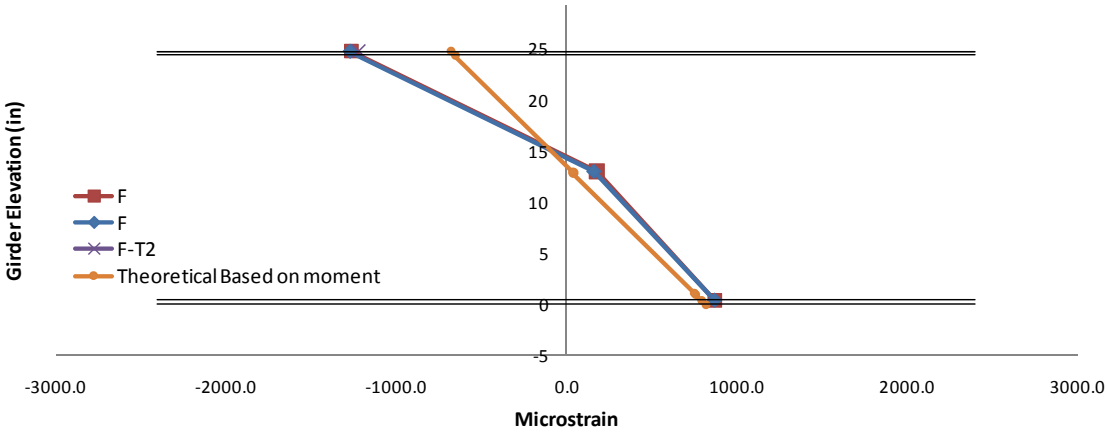

Figure 3-33 Section F strains at three times construction loads

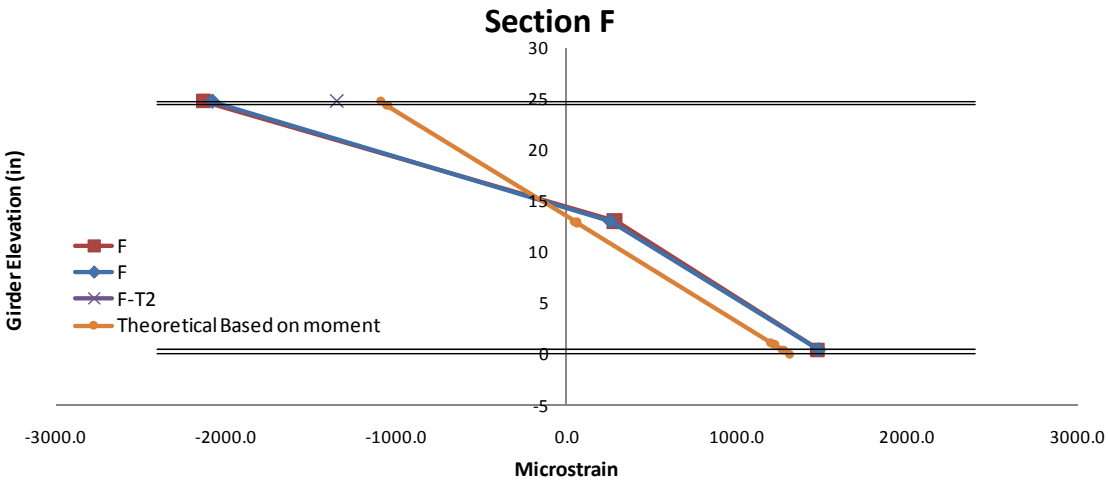

Figure 3-34 Section F strains at ultimate loading

Although the some of the strains are getting close to yielding, buckling is the dominant cause in failure.

3.3 Test B1 Results

Specimen B was tested following the procedures described in the previous chapter. The same load configuration was used for Test B1. Figure 3-35 shows the test setup for the second test. Unlike the first test, no tie plates were removed during testing. After observing how the first girder failure was driven by stress concentrations at the load points, stiffener plates were welded inside the second girder at the load points.

Figure 3-35 Folded plate girder test B1 setup

This section will examine the results from the second ultimate test, starting by looking at the overall performance of the girder and then looking at the performance of specific components of the girder including the performance of the tie plates and the affect they

have on girder behavior, and the strain distributions throughout the girder during testing. Throughout this section, data from the two tests will be compared to show differences from the two tests.

Figure 3-36 shows the moment deflection graph for Both Test A1 and Test B1. The graph contains data from vertical pots. The green line represents the maximum amount of moment that would be experienced during construction. The curves in the graph are from pots that were located at the mid-span of the specimens.

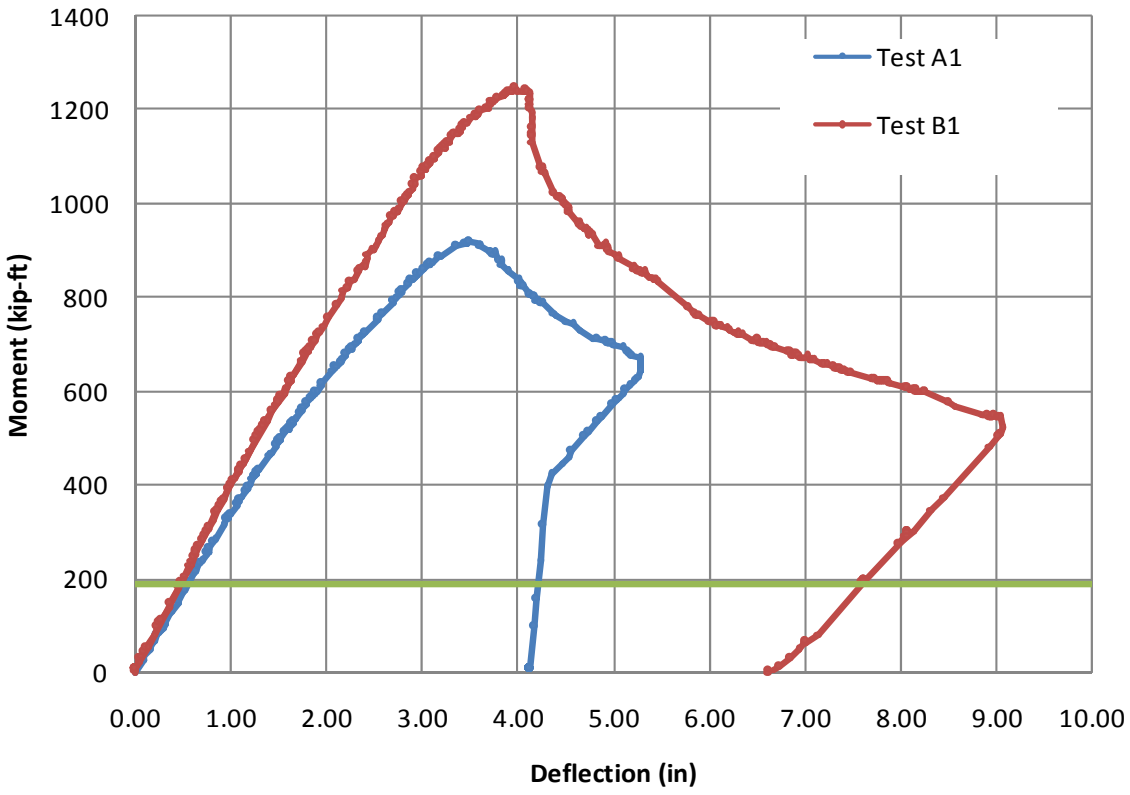

Figure 3-36 Moment deflection curves from the two tests

Both specimens deflect linearly up past the construction moment. The second girder showed greater stiffness that the first. This was the result of a couple of things. The

stiffener plates at the load points prevented the deformation of the top flange. In addition, the presence of tie plates maintains the girder geometry during loading which increases stiffness. Both girders deflect linearly up past the construction moment and up to roughly 2 times the construction moment. After this, the first specimen begins non-linear behavior while the second specimen maintains nearly linear behavior up past 1000 kip-ft, which is more than 5 times the construction moment. The second specimen reaches a much higher ultimate moment but also fails more abruptly.

The following figures will show the deformation of the girder throughout loading. Figure 3-37 shows the top flange at two times the construction moment.

Figure 3-37 Top flange at twice the construction moment

The top flange is beginning to buckle slightly. The leaning shear studs are the best indicator of the top flange deformation.

Figure 3-38 Test B1 at 106 kip

Figure 3-39 shows the top flange at 120kips; the deformation of the top flange is becoming more apparent. Figure 3-40 through Figure 3-43 show different parts of the beam at 140kips of load. This is within five kips of the ultimate load, when the girder begins to fail. Figure 3-41 shows that the deformation of the girder is actually bending the tie plate. Figure 3-42 is a picture taken from the west end of the girder looking down the top flange towards the spreader beam. Near that spreader beam, the top flange is buckling downwards. Figure 3-43 shows the deformation of the top flange between the load points.

Figure 3-39 Test B1 top flange at 120kip

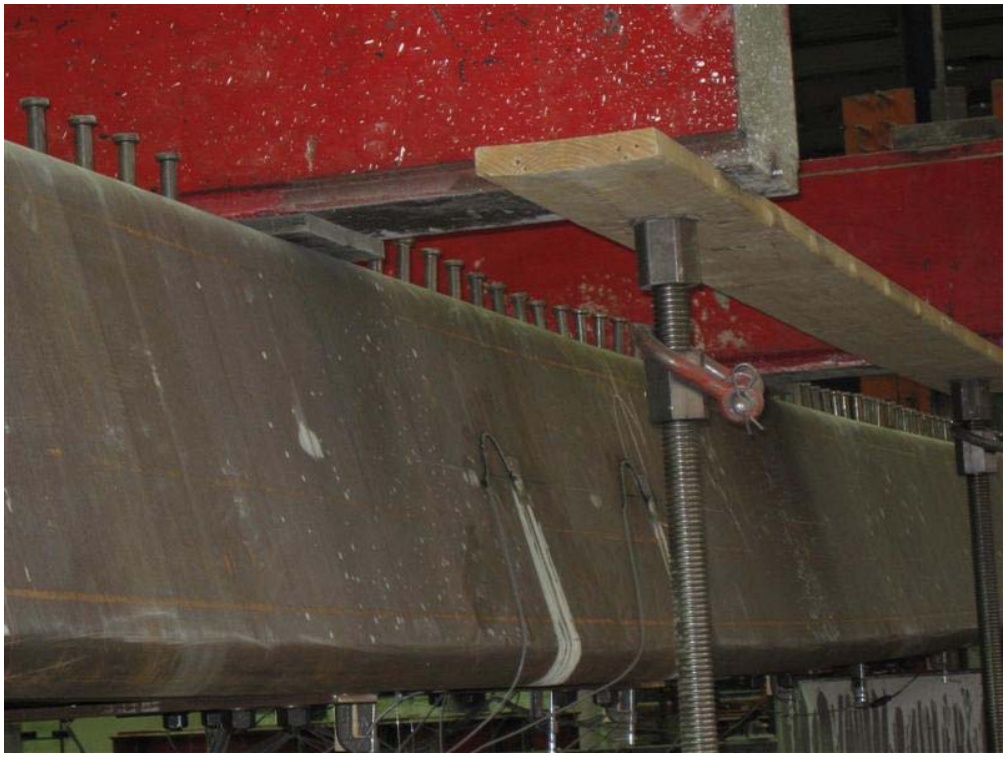

Figure 3-40 Test B1 web at 140kip

Figure 3-41 Test B1 tie plate at 140kip

Figure 3-42 Test B1 top flange at 140kip

Figure 3-43 140kip

Shortly after these pictures were taken the girder reached its ultimate capacity and began to fail. Figure 3-44 shows the top flange when loading is at 137kips as the girder continues to fail. Figure 3-45 shows the girder outside of the load points also at 137kips.These two figures show a difference in the amount of buckling taking place in between the load points compared to outside of the load points.

Figure 3-44 Top flange at 137 kip after failure

Figure 3-45 Girder outside load points at 137 kip on way back down

After the girder was unloaded, pictures were taken of the final deformed shape of the specimen. Figure 3-46 shows the overall girder deformation after unloading. The

extreme buckling at midspan resulted in what was almost a hinge. The midspan area contained most of the permanent deformation; the rest of the girder returned to its original state. Figure 3-47 shows the girder on both sides of the west load point. This picture also shows that the majority of the failure occurred at midspan. Figure 3-48 shows the section of the girder between load points and Figure 3-49 provides a closer view of the web buckling.

Figure 3-46 Girder deflection after unloading

Figure 3-47 Permanent deformation after unloading

Figure 3-48 Girder deformation at midspan of girder after unloading

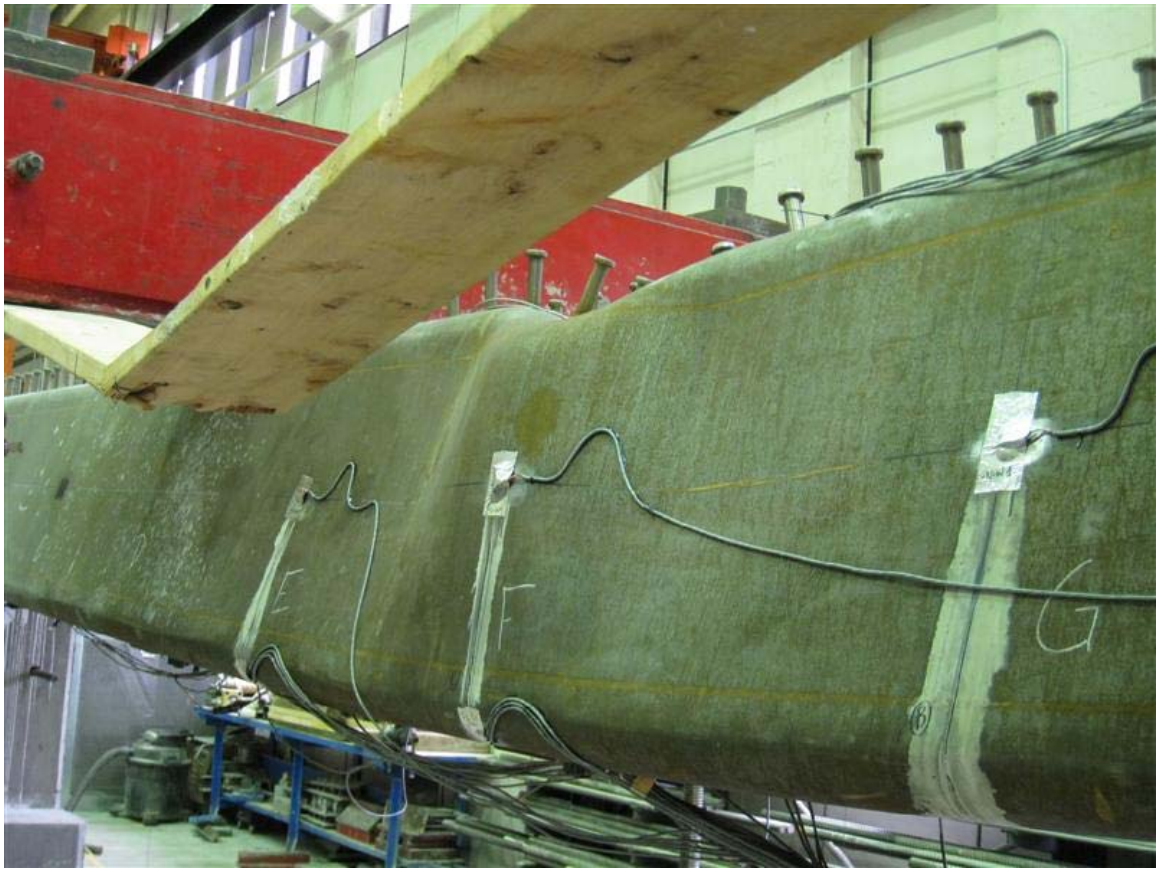

Figure 3-49 Girder permanent deformation after unloading. Web buckling

In summary the following graph, Figure 3-50, shows where the pictures fall within the loading of the girder.

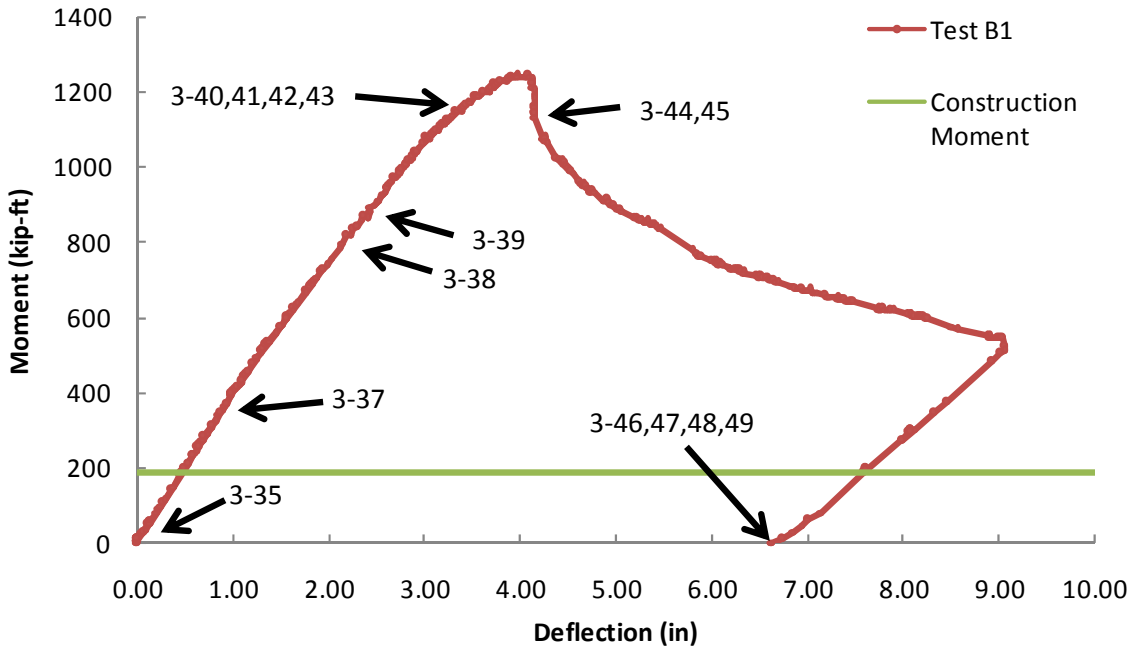

Figure 3-50 Figure labels showing time at which photos were taken

The result of the added stiffener plates was a shift from local deformation at the load points to a more general deformation in the top flange along the length of the beam. The failure in the first test was crushing of the girder. The failure in the second test was buckling from flexure.

Tie plate performance is covered in the following paragraph. Unlike the first girder tested, where some tie plates were removed during testing, all tie plates remained place throughout testing of the second specimen. The stiffener plates installed at the load points aided the tie plates in resisting flange separation and maintaining the girder's shape. Figure 3-51 shows the bottom flange separation data that was measured using pots.

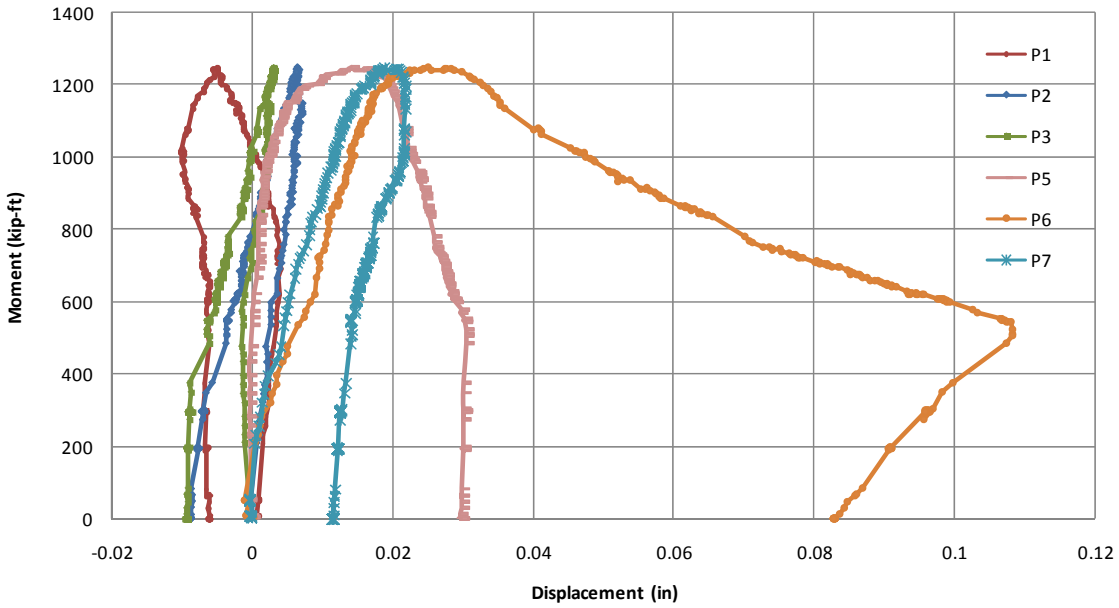

Figure 3-51 Flange separation moment-displacement graph

The stiffener plates that were present at the load points provided bracing to the girder that assisted the tie plates at section D and section H. At the construction moment, the largest flange movement was at mid-span and that was 0.0012 inches. Even up to ultimate capacity, all flange separation was less than .02 inches. Figure 3-52 shows the moment vs. strain curve for the tie plates at section F and D for the second test. At the construction load moment of 187 kip-ft, the strains in both tie plates are less than 25 micro strain. That is about 1% of the yield strain of the steel. The strains in the tie plates are in opposite directions. The flanges at section F are trying to separate while the flanges at section D are trying to come together. The stiffener plates create a point in the girder that acts like a support. On one side of the support, the flanges are separating and as a result, the flanges on the other side are moving in the opposite direction. The graph also shows that when the girder fails, the buckling can greatly

affect the force resisted by the tie plates. Figure 3-41 showed the tie plate at section F bending because of the girder deformation. This flexure creates secondary strains in the tie plate which can dominate the strain at the bottom of the tie plate. If a second gage was located on the top of the tie plate, the combined strain from flexure and tension would create total strain that would be much larger than what is shown in the curve for F-P.

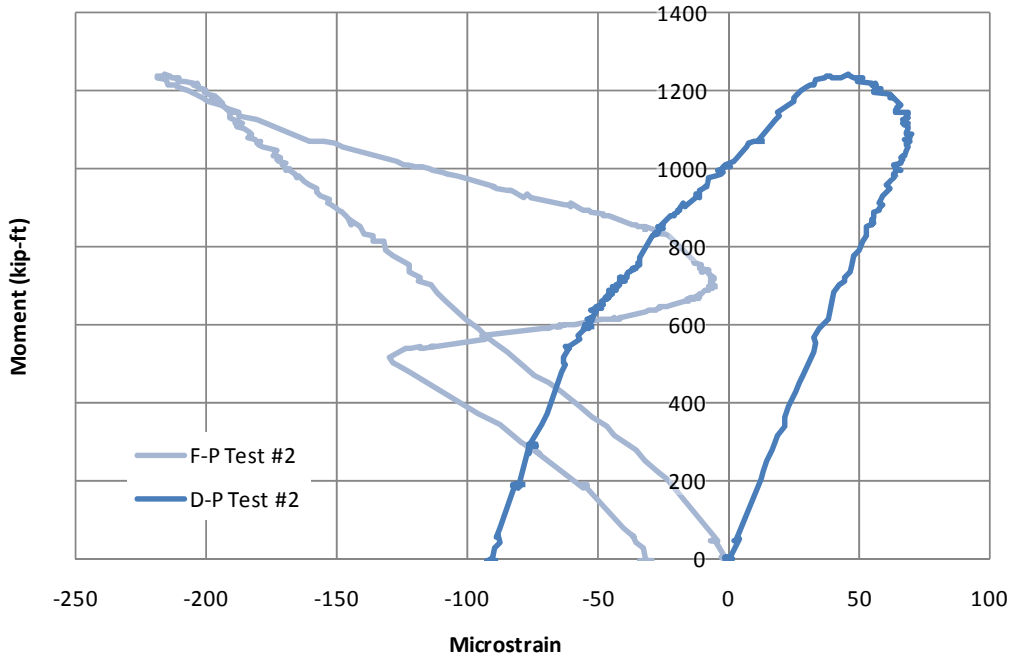

Figure 3-52 Moment vs. strain data for tie plates at section F and D

Figure 3-53 Compares data from the same tie plates in the two different tests. The only difference between the two tests at this point is the presence of stiffener plates at the load points. The data shows that the stiffener reduces the stress that the tie plates experience during loading by both holding the flanges in place and reducing the buckling

of the top flange, which is the primary cause of separation of the flanges. The data also shows that the tie plates are the reason that the strains are in the opposite direction in test B1.

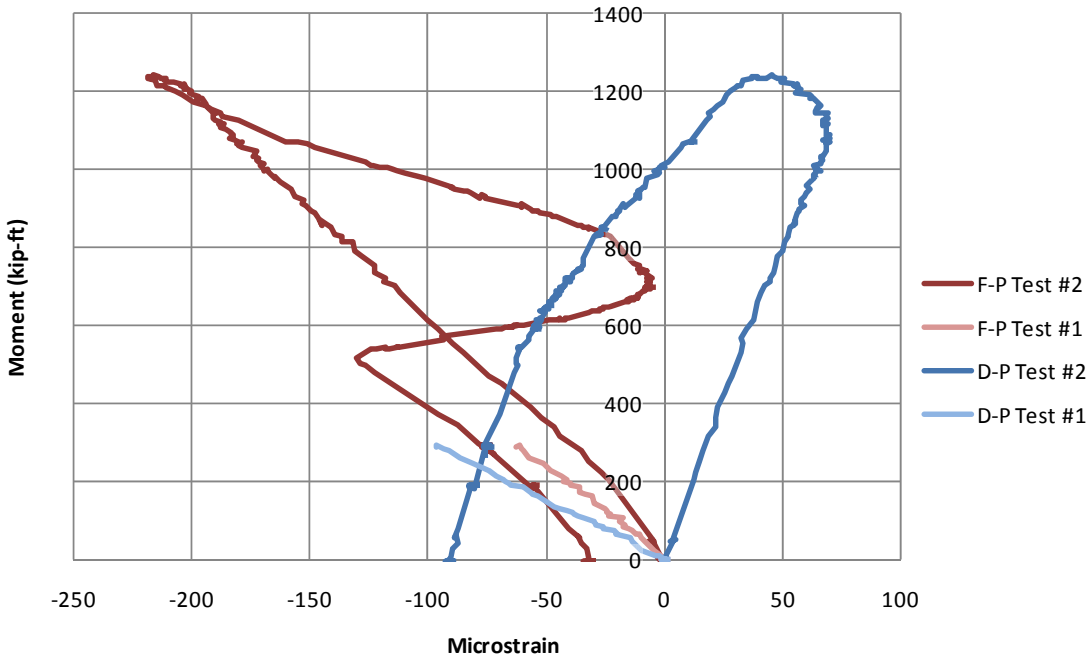

Figure 3-53 Comparison of tie plate strain data from Test A1 and Test B1

The following figures show the progression of the strain distribution throughout loading for test B1. Strain gage data from section E, F, and G is shown. Theoretical strain distribution based on the applied moment is shown in orange to give reference. The first strain distribution, Figure 3-54, is at a moment of about 200 kip-ft, which is close to the calculated construction moment. The strain data matches well with the theoretical data.

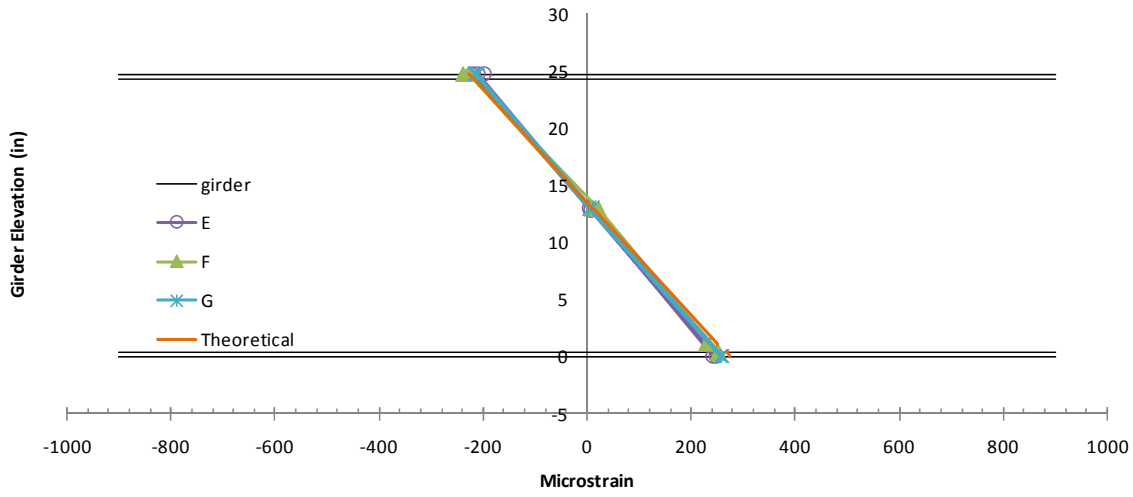

Figure 3-54 Strain distribution at construction moment

The strain distribution in Figure 3-55 is at double the construction moment and has predictable results. The strain distribution shown in Figure 3-56 is at 3 times the construction moment. None of the strain distributions are falling on the theoretical line anymore. The bottom flange strains are still close, but the web and top flanges are not. E and G match each other, and F is behaving opposite of those two. Remember that F is at mid-span and E and G are symmetric and located on both sides of F.

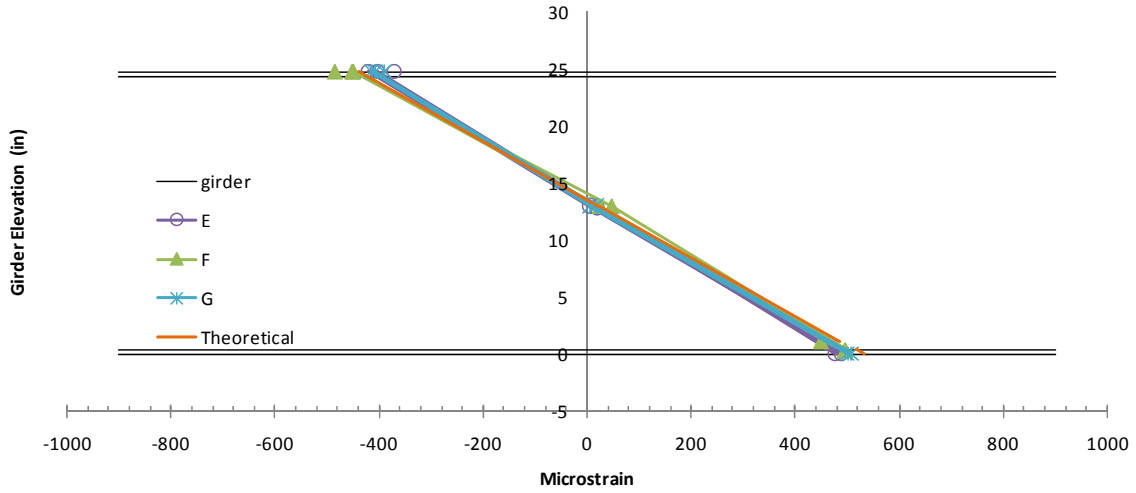

Figure 3-55 Strain distribution at two times the construction moment

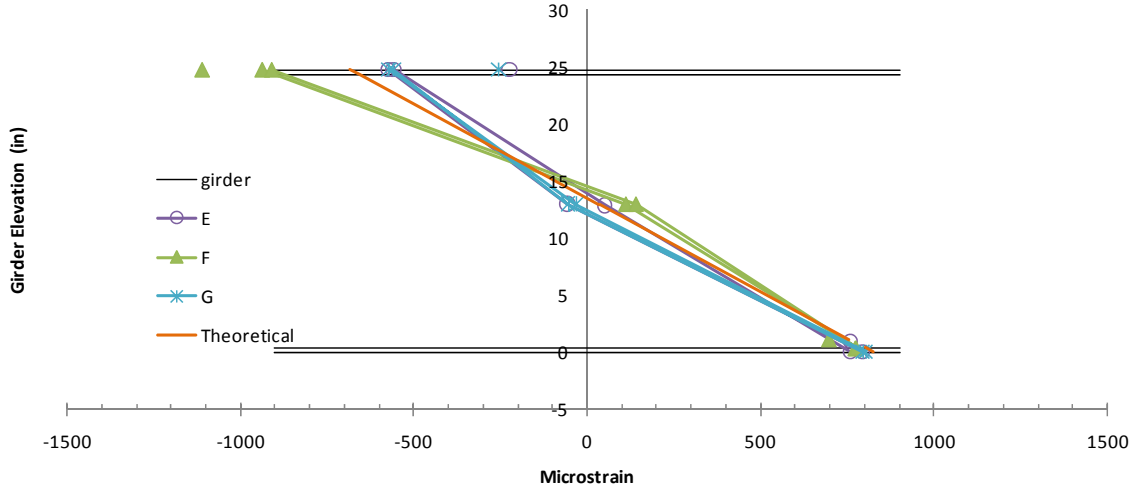

Figure 3-56 Strain distribution at 3 times the construction moment

Figure 3-57 and Figure 3-58 show the strain distributions at four and six times the construction moment respectively. The top flange and web strains continue to deviate farther from the theoretical as load and the resulting buckling increase. Something in the bottom flange strain gages at section F changes drastically between Figure 3-58 and Figure 3-59, which shows the strain distribution at ultimate load. Figure 3-60 shows the

strain distribution at the highest deflection before unloading, and Figure 3-61 shows the strain distribution or permanent deformation after unloading.

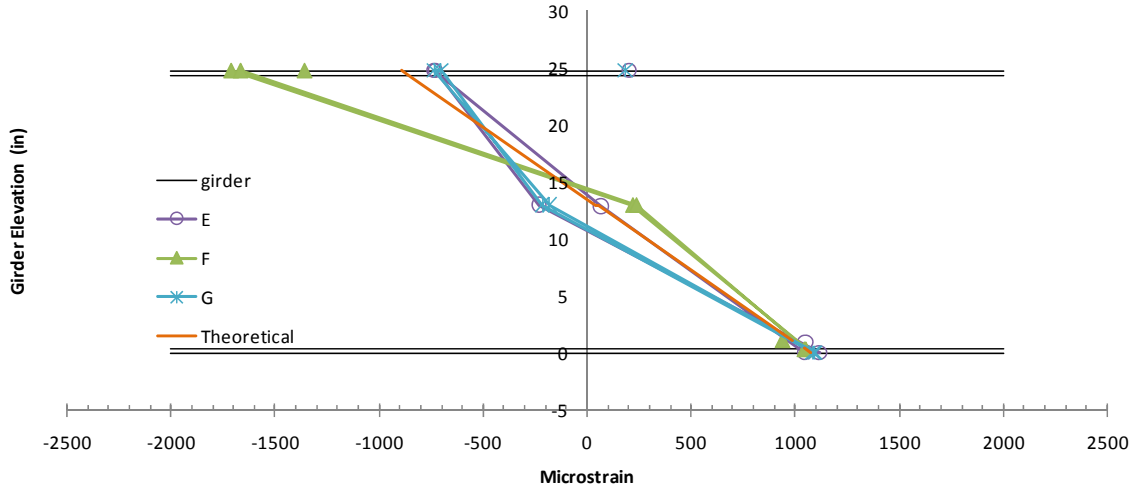

Figure 3-57 Strain distribution at 4 times the construction moment

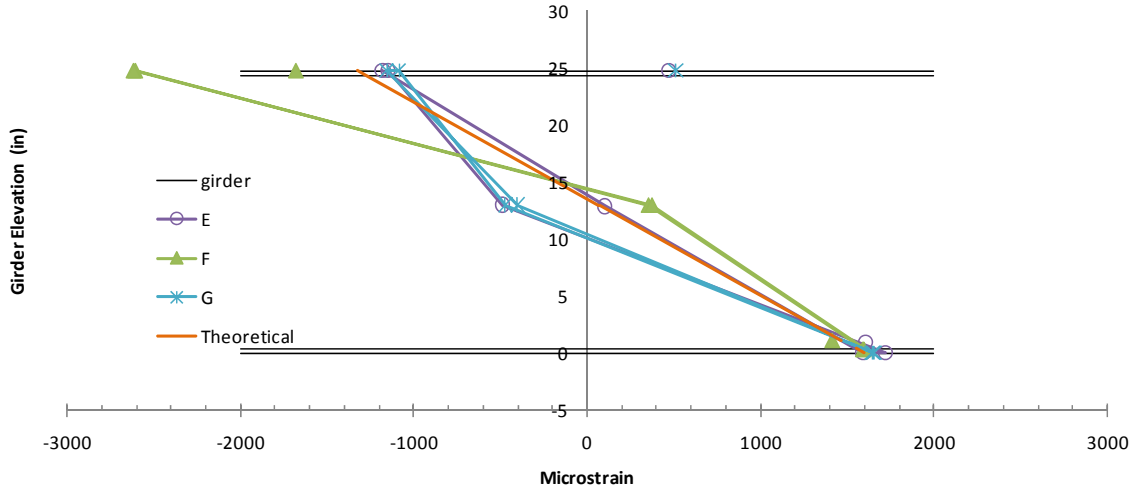

Figure 3-58 Strain distribution at 6 times the construction moment

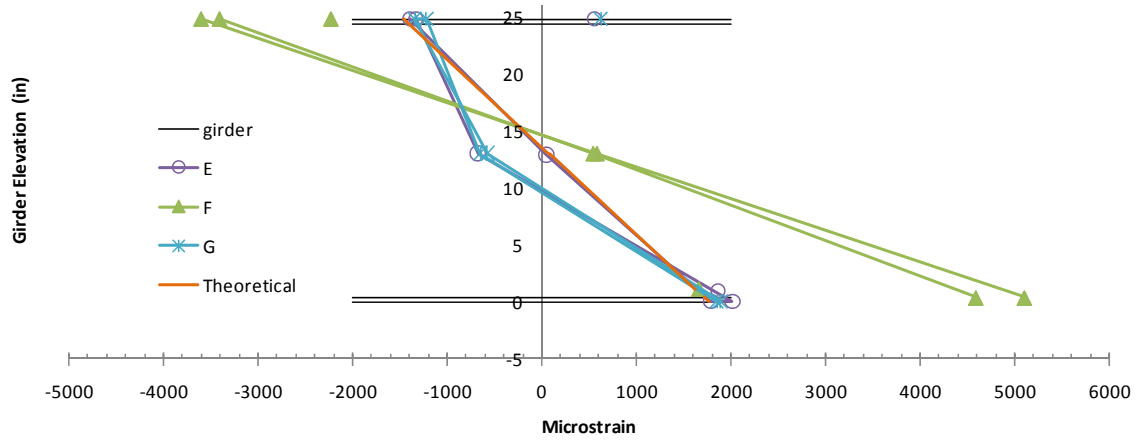

Figure 3-59 Strain distribution at ultimate moment

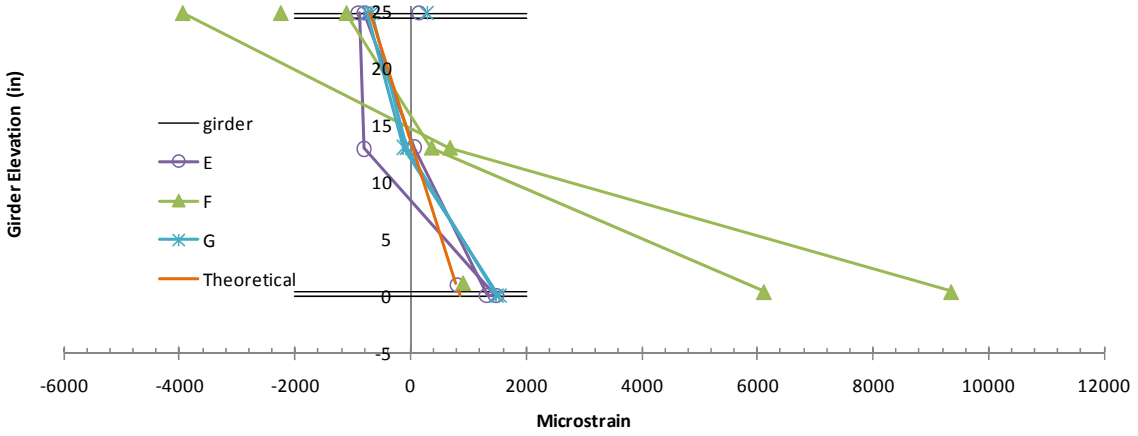

Figure 3-60 Strain distribution at 614kip-ft. just before unloading. At ultimate deflection

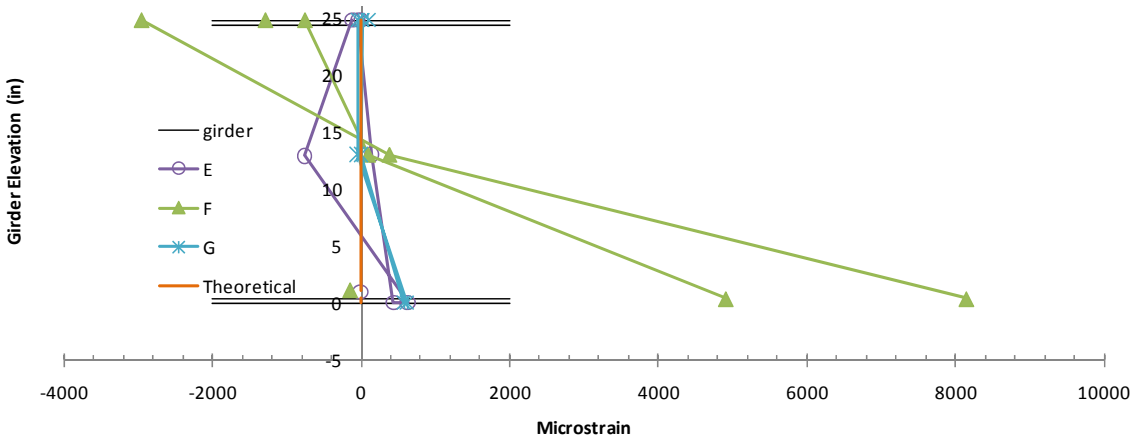

Figure 3-61 Strain distribution after unloading

The cause for the strain discrepancies in the top flange and web is due to the top flange starting to buckle. When the top flange buckles, the webs also are affected. If the top flange goes down the webs go out and if the top flange goes up the webs go in as illustrated in Figure 3-62.

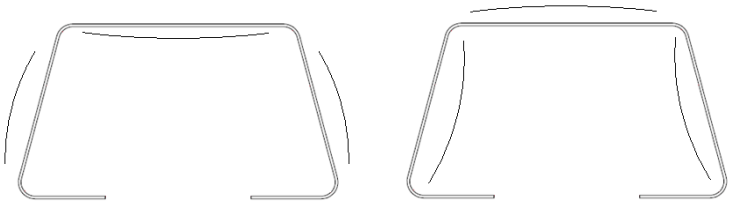

Figure 3-62 Girder deformation illustration

This results in strains that are either high in the top flange and low in the web or low in the top flange and high in the web. This can be seen in the strains of section E and G and opposite for section F starting in Figure 3-56.These deformations did not affect the strains in the bottom flanges.

It can be seen that the bottom flange strains match quite closely to the theoretical strains throughout loading. The exception is the bottom flange data from section F. Near ultimate loading the strains in the bottom flange grew very quickly. To better see what is happening at these gages, look at the following figures of load and strain vs. time and load vs. strain. Figure 3-63 shows the strain (primary axis) on the left and loading (secondary axis) on the right vs. time on the horizontal axis for the strain gages located at the bottom of section F. After the 4800 second mark the strains in the two flanges begin to grow very quickly each time that load is applied, while the strains measured at the rosettes, which were located only slightly higher in the girder elevation,

continue to grow at a pace displayed earlier in testing. Figure 3-64 shows moment vs. strain for the same gages. It can be seen near the peak loading that the bottom flange strain gages, FN-B1 and FN-B2, measure large additional strain for small amounts of additional load. This graph also shows the strain data from the rosette strain gages which display linear behavior in spite of their location with respect to FN-B1 and FN-B2. Figure 3-65 shows the moment vs. strain relationship at the bottom flanges of sections E and G. Even though those sections experienced the same moments as section F, the same behavior was not seen at section E and G.

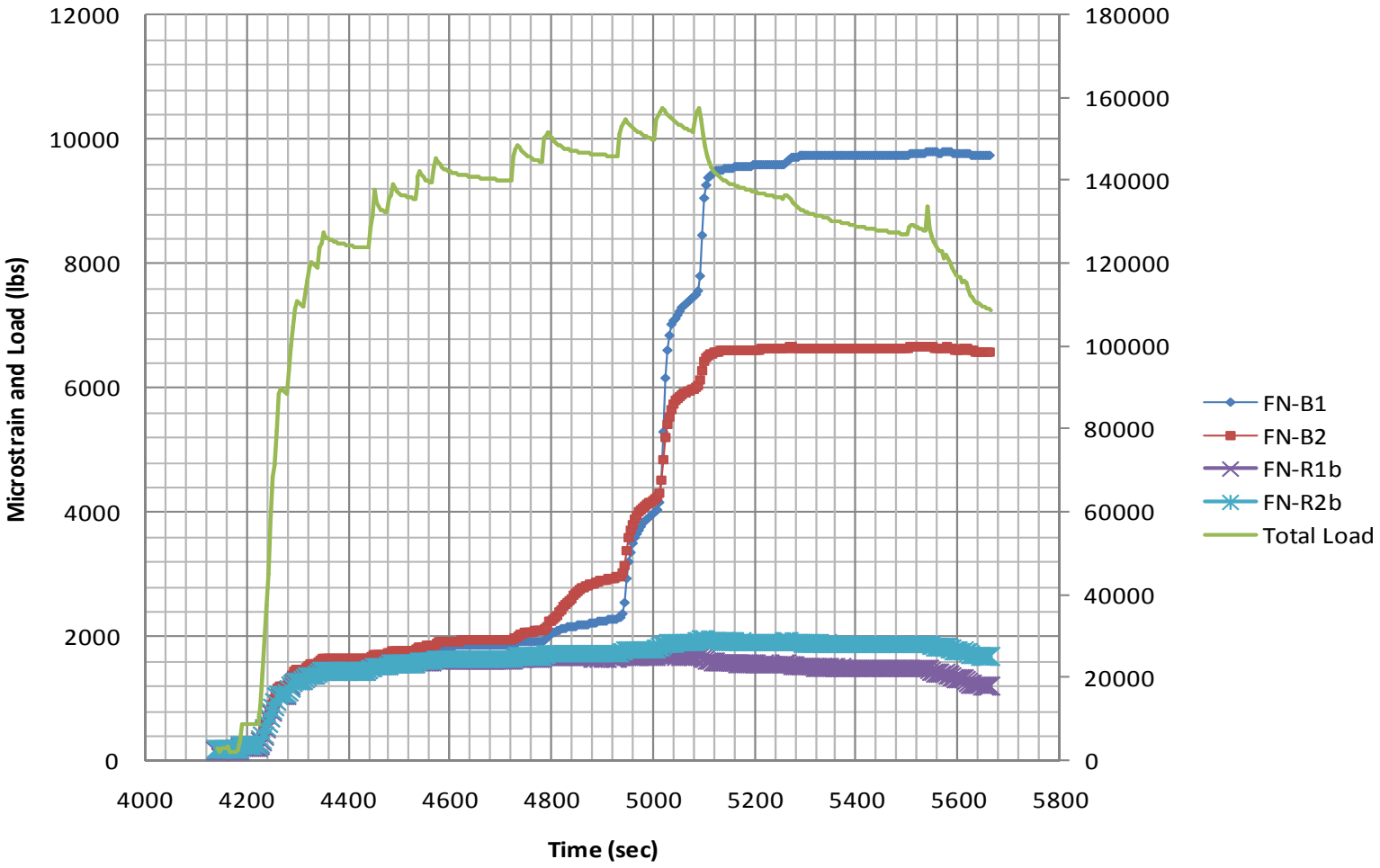

Figure 3-63 Load and strain data history

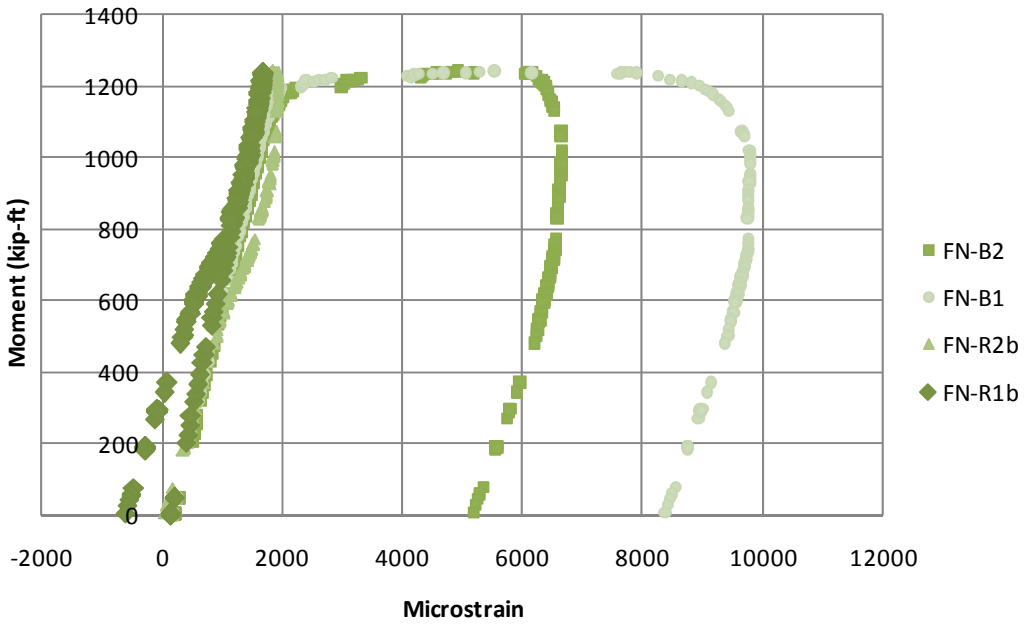

Figure 3-64 Moment strain relationship at bottom of section F

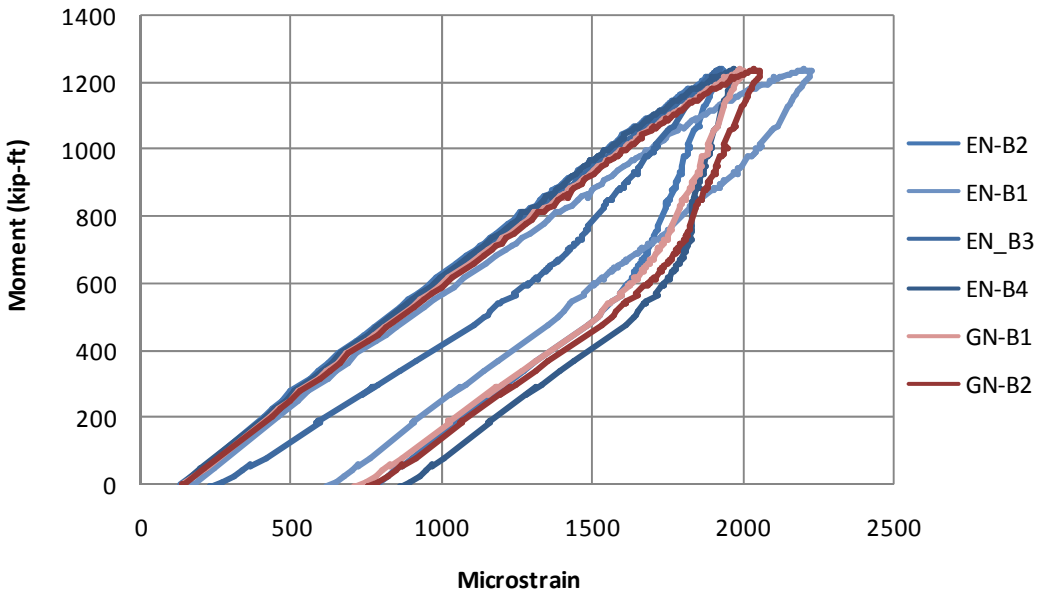

Figure 3-65 Moment Strain relationship at bottom of sections E and G

There could be a couple of explanations for this behavior at the bottom flange of section F. First the strain gages, FN-B1 and FN-B2, could have failed. The other explanation would be that the flange experienced yielding at these locations.

There are two main ways that strain gages can fail during loading. The adhesive that bonds the gage to the steel can fail resulting in a drop in the strain in the gage which is not the case in this situation. The other way a strain gage can fail is that the foil matrix can fail which would cause an increase in the resistance of the gage and as a result an increase in the strain reading. This is a possible explanation for the unusually large strains. The large difference in the strains in the bottom flange compared to the bottom bend of the girder provides some argument for the strain gage failure. Also the strains at sections E and G were at similar levels but did not show the same behavior.

There are several things that indicate that yielding could be happening. First, the strain at which this occurred, was very close to the stain where yielding began during the material testing from girder samples. Second, the presence of a tie plate, located at section F and not at sections E and G, could be the cause of the difference. Third, the girder failure, extreme buckling and deformation, occurred at section F. Finally, the fact that the two strain gages in question, which were located symmetrically on opposite flanges, showed very similar behavior at the same load levels, seems to point toward yielding as being the cause of the high strains at section F. It seems unlikely that the two gages would fail at the same point while all of the gages located at section E and G did not fail at similar strain levels.

Chapter 4

Conclusions

The following sections summarize the constructability testing of folded plate girders A1 and B1, and present the conclusions of the research.

4.1 Summary

Constructability testing of two folded plate girder specimens was performed. Both girders were tested over a simple span with two symmetric load points. The girders have tie plates between the bottom flanges to control flange separation. During the first test, three tie plates were removed for part of testing so that the effect of their presence could be observed. During the second test, the tie plates remained in place throughout loading. Also during the second test stiffener plates were added at the load points to eliminate the local deformation that resulted from the concentrated loads.

During construction the majority of the load on the girder would result from the pouring of the concrete deck which is a distributed load. Also, the load during construction is not restricted to the top flange. The hangers that hold the formwork in place during construction distribute some of the construction loading to the sides of the girder near the bottom of the web. Therefore, the use of point loading to reach ultimate capacity results in conservative results.

The goal of testing was to evaluate both the overall girder performance while also testing the girder components' performance. The girder was tested not only to see how it performs at construction loading, but also to see what load levels cause failure and what the mode or modes of failure are.

4.2 Conclusions

Results of the two tests reported in this thesis are part of ongoing research in the folded plate girder system being developed at the University of Nebraska. Therefore the conclusion statements presented in this thesis are limited to the constructability testing mentioned herein.

Both specimens that were tested displayed stability and ductility though all stages of testing. There were no undesirable, visible or measurable, deformations in the girder at moments equivalent to those experienced during construction.

Tie plates perform a key function by maintaining the girder shape during construction, when the girder is most vulnerable to deformation. Testing confirmed that the tie

plates are both necessary and effective for preventing flange separation at construction load levels and both flange separation and rotation at higher load levels, which cause deformation and buckling in the girder. More evaluation of the tie plates will be necessary to determine the optimum tie plate configuration.

The top flange of the folded plate girder experiences the highest stress during construction. After construction of the deck is complete and the concrete is hardened, the neutral axis is shifted up near the interface between the top flange and deck. At this point, the top flange will experience little stress because it is located close to the neutral axis of the composite beam. The top flange was the weakest component of the beam during construction due to its role as a compression element that has a slender and un-braced form. The compression in the top flange caused local buckling in the top flange even at elastic load levels. This was the cause for loss of stiffness and failure in both specimens. The addition of local deformation that resulted from stress concentrations to the buckling that occurs from compression of the top flange reduces both the stiffness and the ultimate capacity of the girder. This is shown in the difference in performance between Test A1 and Test B1.

Incorporation of a ridge at the center of the top flange of specimens, results of which are not reported in this thesis, proved to resolve this very early buckling issue.

5 Bibliography

AASHTO. (2007). *AASHTO LRFD Bridge Design Specifications, 4th ed., American Assiciation of State Highway and Transportation Officials.* Washington, D.C.

ASTM A370 - 09ae1 Standard Test Methods and Definitions for MEchanical Testing of Steel Products.

FHWA NBI data. (n.d.). Retrieved from http://www.fhwa.dot.gov/bridge/nbi/.

Galambos, T. V. (1976). *Guide to Stability Design Criteria for Metal Structures.*

SSRC Technical Memorandum No. 7: Tension Testing. (1986).